RADIO FREQUENCY DOSIMETRY IN THE CRAWFORD CELL BETWEEN 400 AND 500 MEGAHERTZ

BY

RAJU CHANDRA

B.S., University of Illinois, 1981

THESIS

Submitted in partial fulfillment of the requirements
for the degree of Master of Science in Electrical Engineering
in the Graduate College of the
University of Illinois at Urbana-Champaign,1983

Urbana, Illinois

ACKNOWLEDGEMENTS

The author would like to express gratitude to his advisor Dr. Richard Magin for his encouragement,guidance and patience throughout the course of this thesis. Special thanks are also due Dr. Charles Cain for providing the author an opportunity to work in this area. Secondly, thanks are due to the entire staff at the Bioacoustics Research Lab for providing incredible support during the course of this thesis. Specifically, thanks are due to Mr. Bill McNeil for his help in constructing the Crawford Cell and animal cages, Mr. Joseph Cobb for his invaluable assistance in setting up the exposure facility, Mr. Michael Haney and Mr. Steve Foster for their assistance in solving software problems, Dr. Ronald Johnston for his keen insights in discussions and Mrs. Wanda Elliot for her totally unselfish secretarial work. Finally the author would also like to thank his parents for all the love and support they have given him.

TABLE OF CONTENTS

CHAPTER I

INTRODUCTION

The purpose of this study is to develop an exposure system to investigate the effects of electromagnetic waves on small animals. There is presently some controversy regarding the safety limit of electromagnetic energy that is harmful to man. Scientists in the USSR have set an incident power density level of .01 mW/cm*cm (1), which they consider as the maximum safe exposure level for man. Meanwhile,in the United States the maximum safe level of exposure is at 10 mW/cm*cm (2). In this study we will describe a microwave exposure chamber that can be used to conduct research to investigate this discrepancy. We report dosimetry studies on hamsters and their prolate spheroidal models in an attempt to better understand the absorption of electromagnetic energy by small animals. This study is a part of an effort currently taking place at the University of Illinois and other institutions to study this problem.

Research work in the area of radio frequency absorption can be divided into two areas - theoretical and experimental. The theoretical work has been directed towards finding the electromagnetic fields inside biological bodies under assumed illumination. Knowledge of the internal fields and the dielectric properties immediately gives the power absorbed by the biological body, which is the parameter of most interest. Biological bodies are usually modeled as lossy inhomogenous

dielectrics. Lin, Guy and Johnson have found the fields in spheroidal models of man when the incident illumination is a plane wave (3). Johnson, Durney and Massoudi have found the internal fields when the incident illumination is a plane wave and the lossy dielectric is modelled as an ellipsoid or a prolate spheroid (4-5). Livesay and Chen (6) and the Food and Drug Administration (7) have found the internal fields when the incident illumination is a plane wave and the lossy dielectric is of a arbitrary shape. Lakhtakia and Iskander have calculated the fields when the lossy dielectric test object is in the near field of a source (8). Ruppin has found the fields inside prolate spheroids using a point matching technique, which extends the frequency range over which the equations are valid (9). Recently, a new approach developed at the University of Illinois specifically for finding the fields from complex scatterers has been published (10). Initial indications on this Spectral Iterative Technique look promising. An overview of the current state of the art in theoretical techniques has been done by Durney (11).

Experimental research work has concerned itself primarily with measuring the whole body absorption of the test object. Because most of the published work has assumed plane wave illumination, it is desirable to expose the test object to a transverse electromagnetic wave. Hill has done whole body absorption studies in a TEM cell on humans and their prolate spheroid models (12). Marshall et al. have done whole body absorption studies on mice (13). Gandhi has also done whole body

power absorption measurements in both free space (14) and in a parallel plate waveguide (15-16) system. He found that absorption depends strongly on polarization and frequency. Iskander et al. have done whole body power absorption measurements on spheroidal models exposed to a near field of a source (17). The basic limitation with free space exposure systems is an inability to accurately measure power absorbed by the test object, which explains the popularity of TEM cells for radio frequency absorption studies. An excellent overview on the state of the art in measurement systems has been done by Weil and Kinn (18). Finally, for eventual use in clinical hyperthermia, it is desirable to focus the electromagnetic energy so that it heats the tumor only. Some electromagnetic focusing systems have been reported (19-20). However, before using these systems local (as opposed to whole body) absorption must be fully understood.

It has been shown in the literature that expressing the safety limit of electromagnetic power absorption in terms of only the incident power density may not be sufficent (21-23). Frequency, polarization,geometry of the absorber and its weight all play a very important role in determining the quantity of absorbed power. Therefore, Johnson and Guy proposed that the quantity of absorbed power be normalized to the volume of the tissue.This then defines a Specific Absorption Rate (SAR) which has units of W/kg. Going one step further, the power absorbed can be normalized to the incident power density level. This then defines a Specific Absorption Rate Normalized (SARN) which has units of W/kg per mW/cm*cm. Since this would account for varying

levels of incident power, SARN will be used in this thesis as a common denominator for comparing dosimetric results of different objects.

CHAPTER II

THE EXPERIMENTAL SYSTEM

A. Description of the System

In deciding upon the exposure facility, it was desired to have the incident energy on the absorber to be in the form of a Transverse Electromagnetic (TEM) wave, so that the absorber could be modeled to be in the far field of an antenna. Mathematical modelling of the fields inside the absorber is then greatly simplified. Comparison of the results to those published then becomes much simpler (24). For this purpose a Crawford Cell exposure system was developed. Alan Segal in his Master's thesis designed and characterized the system that will be used in this study (25). We will expand on his work and do more detailed dosimetry on phantoms in the 400 to 500 MHz range and also do dosimetry on hamsters. The exposure facility is a coupled parallel plate waveguide system that is in a shielded anechoic chamber.A diagram of the Crawford Cell is shown in Figure 2-1. This exposure system is similiar to a tri-plate TEM transmission line discussed by Gandhi. (26)

The coupled parallel plate rectangular waveguide system is called a Crawford Cell in honor of M. L. Crawford who first developed it at the National Bureau of Standards for the purpose of radio frequency dosimetry (27). In a later paper he

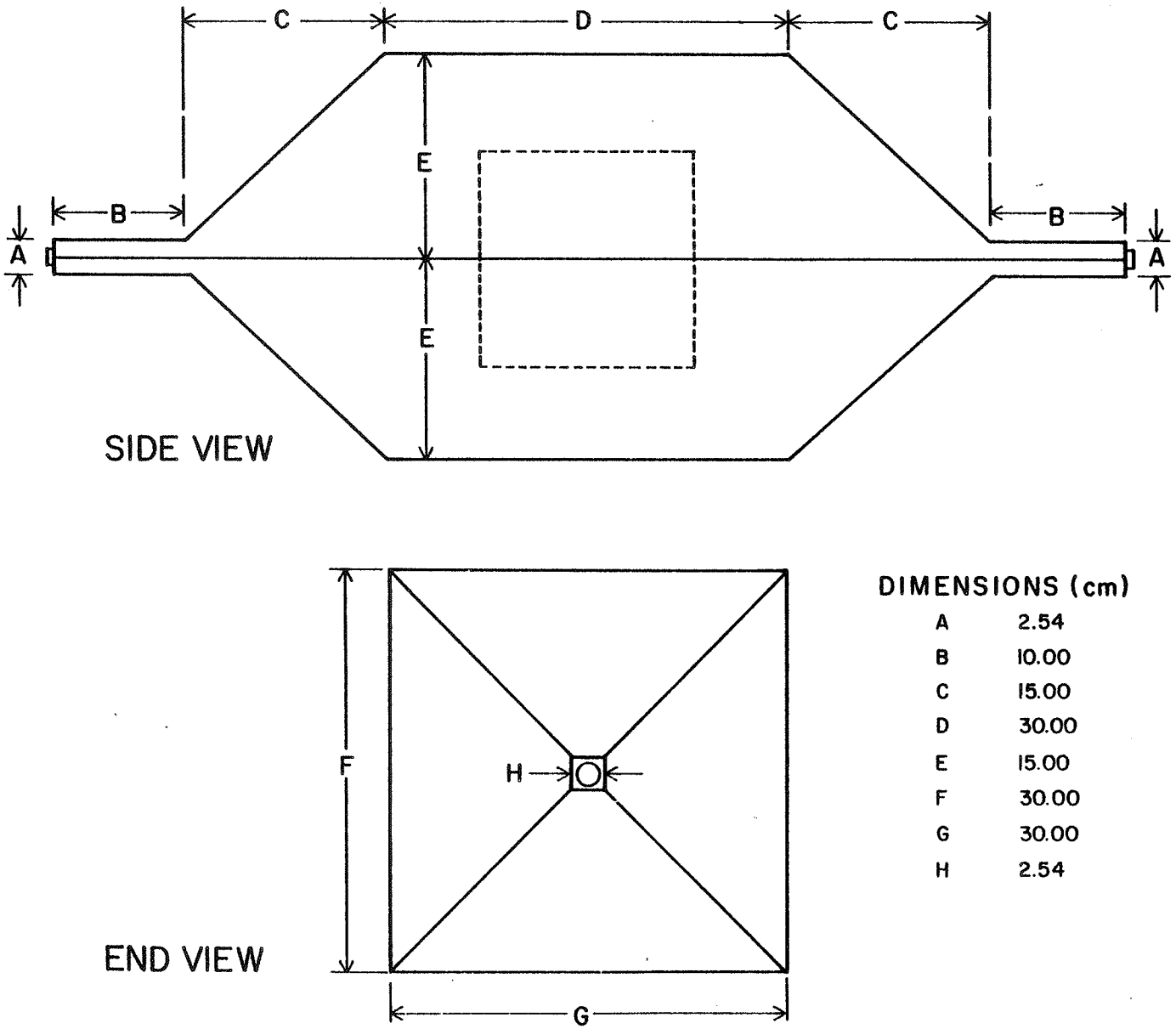

Figure 2-1. Dimensions of the Small Crawford Cell.

developed equations for the impedance,cutoff frequencies of the different modes and resonance frequencies of the Crawford Cell (28). Those equations for the first higher order mode ,i.e., TE_{10} are

$$f_c\,(MHz) = \frac{75}{a}\sqrt{1+\frac{4ab}{\pi b_1 b_2 \ln\frac{8a}{\pi g}}}$$

where a,b,d,b_1,b_2,g and w are defined in Figure 2-2 and

$$f_{RES}\,(MHz) = \sqrt{f_c^2 + \frac{c^2}{2d}}$$

$$Z_0 \cong \frac{\eta_0}{4\left[\frac{a}{b} - \frac{2}{\pi}\ln\left(\sinh\frac{\pi g}{2b}\right) - \frac{\Delta c}{\varepsilon_0}\right]}$$

$$\eta_0 = 377\,\Omega$$

where $\Delta c/\varepsilon_0$ can be neglected.

Two such cells,a large one and a small one, were built. Although it was initially desired to do dosimetry in both cells, only dosimetry in the small cell was done. This is because in the big cell the power density levels were so low that meaningful dosimetric data were unobtainable.

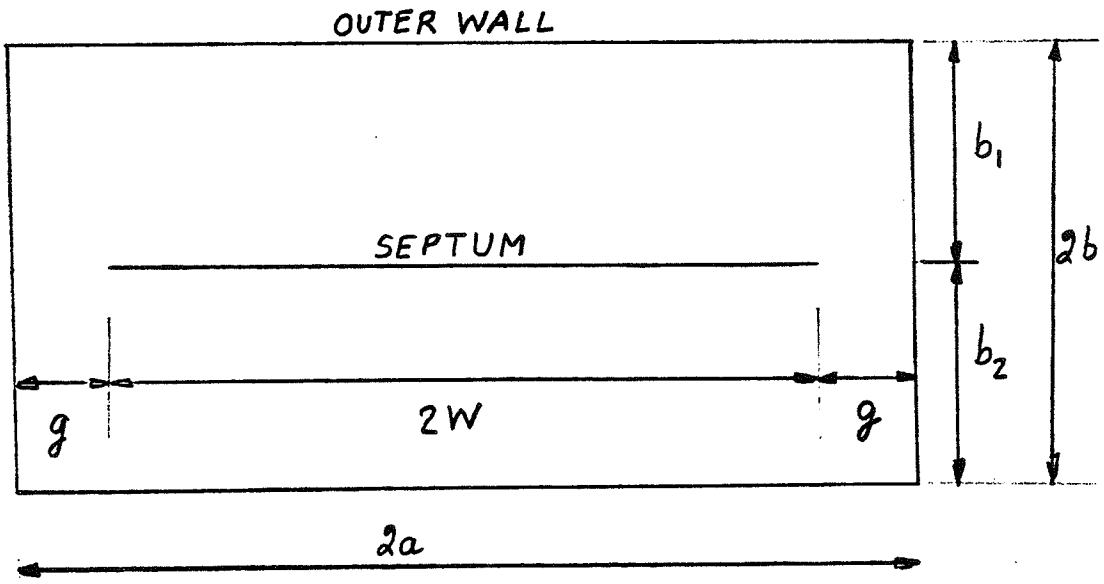

Figure 2-2. Diagram of the Various Parameters Used for Calculating the Higher Order Modes in the Crawford Cell.

For the small cell, the cutoff frequency and the lowest order resonance are

$$2W = 24.924 \text{ cm}$$

$$g = 2.54 \text{ cm}$$

$$b_1 = b_2 = 15.000 \text{ cm}$$

$$2a = 30.000 \text{ cm}$$

$$\therefore f_c(\text{MHz}) = \frac{75}{0.15}\sqrt{1 + \frac{4\times0.15\times0.15}{\pi\times0.15\times0.15 \ln\frac{8\times0.15}{\pi\times0.0254}}}$$

$$= 606.16$$

$$f_{RES}(\text{MHz}) = \sqrt{f_c^2 + \frac{c^2}{2d}}, \quad c^2>0, \ d>0$$

$$\therefore \quad f_{RES} > f_c$$

Hence, if the frequency of operation remains below 606 MHz, only a TEM wave will propagate in the small Crawford Cell. The characteristic impedance is

$$Z_0 \cong \frac{377}{4\left(\frac{0.15}{0.15} - \frac{2}{\pi}\ln\left(\sinh\frac{\pi\times0.0254}{2\times0.15}\right)\right)}$$

$$= 51.346\,\Omega$$

The characteristic impedance of the Crawford Cell is reasonably close to 50 ohms. Again,this is highly desirable as it then allows the Crawford Cell to be connected to the 50 ohm "outside world" without the need for any matching networks. There will be a small mismatch at the input port of the Crawford Cell resulting in some power being reflected back, but that is unavoidable. One can only hope to minimize this power loss (loss because power is reflected and hence does not go towards creating the EM fields inside the Crawford Cell). Although the equations developed by Crawford imply a frequency independent characteristic impedance, this is not the case. It was experimentally determined that the characteristic impedance IS a function of frequency. The Voltage Standing Wave Ratio (VSWR) as a function of frequency was experimentally determined for the system and results are shown in Figure 2-3. It was also experimentally determined (using a Time Domain Reflectometer) (TDR) that Z_o can be taken as a constant along the length of the cell (25).

For the big cell the cutoff frequency is

$$2W = 41.120 \text{ cm}$$

$$g = 4.610 \text{ cm}$$

$$b_1 = b_2 = 25.000 \text{ cm}$$

$$2a = 2b = 50.000 \text{ cm}$$

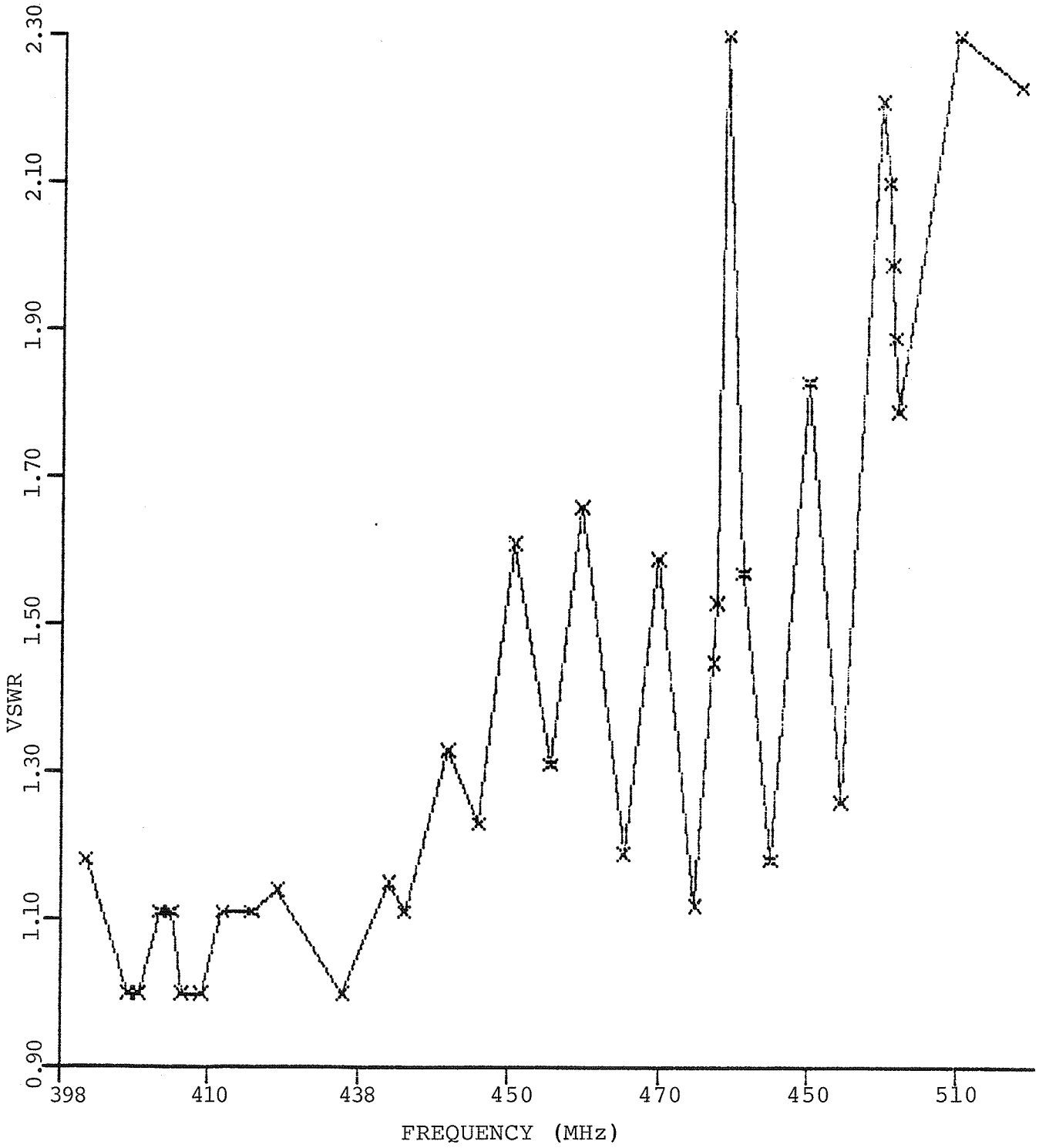

Figure 2-3. Exposure System Frequency Response.

$$f_c\,(\mathrm{MHz}) = \frac{75}{0.25}\sqrt{1 + \frac{4\times0.25\times0.25}{\pi\times0.25\times0.25\times\ln\frac{8\times0.25}{\pi\times0.4604}}}$$

$$= 366$$

Therefore, if the frequency of operation remains below 366 MHz, only a TEM wave will propagate in the big Crawford Cell. The characteristic impedance and resonance frequency are

$$f_{RES}\,(\mathrm{MHz}) = \sqrt{f_c^2 + \frac{c^2}{2d}}\,, \quad c^2>0,\ d>0$$

$$\therefore\ f_{RES} > f_c$$

$$Z_0 \cong \frac{377}{4\left(\frac{0.25}{0.25} - \frac{2}{\pi}\ln\left(\sinh\frac{\pi\times0.04611}{2\times0.25}\right)\right)}$$

$$= 52.956\,\Omega$$

This Z_0 is a little bit worse than the Z_0 for the small cell.

It should be noted that the equations for Z_0 are only valid in the rectangular section of the cell. They should not be used for calculating the characteristic impedance in the neck region of the cell ,i.e., where the rectangular coaxial flares out into a rectangular parallel plate waveguide system. In that region transmission line theory should be used for finding the

characteristic impedance of a coaxial line (26). Hence,

$$Z_0 = 60 \ln \frac{r0}{r1}$$

where r0 is the average radius for the outer square conductor and r1 is the average radius for the inner square conductor. Therefore,

$$\frac{r0}{r1} \cong 2.3$$

achieves $Z_0 \cong 50$ throughout the flare region.

The same principle applies to the output port of the cell as well.

The overall system diagram of the exposure facility is shown in Figure 2-4. Power is being provided by an MGL RF power generator, model # 15222, with a plug-in unit from 400 to 1000 MHz, model # 6050. Only the frequencies from 400 to 500 MHz were looked at extensively. This is because the power generator could not go below 400 MHz, and above 500 MHz the directional couplers, power meters and frequency counter could not function properly. Furthermore, since the cutoff frequency for the TE_{10} mode in the big cell is approximately 366 MHz, which is below what the generator can put out, big cell experiments were effectively by-passed.

From the generator, power goes to a Bird RF power analyst, model # 4381. The plug-in unit for the forward power slot is rated at 200 - 500 MHz and 100 W and the plug-in unit for

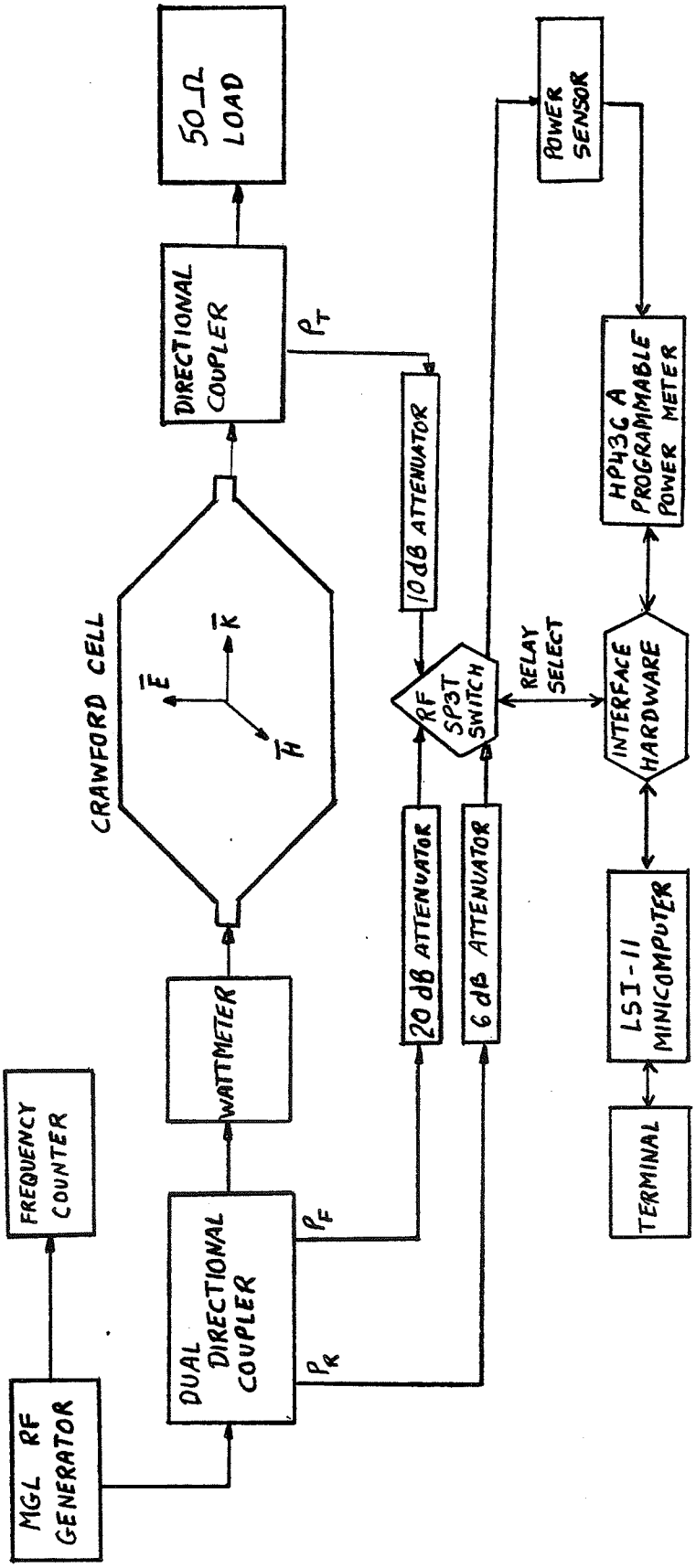

Figure 2-4. Block Diagram of the Crawford Cell Exposure Facility.

the reflected power slot is rated at 200-500 MHz, 10 W. All the transmission lines in the system are Belden RG-8/U 50 ohm coaxial cables. The Bird power meter basically monitors the input power to the system, the reflected power and the VSWR. None of the parameters being displayed by the Bird power meter is directly being used to calculate the SARN of the absorber. The meter only provides a convenient check to the actual data mesurements.

From the Bird power meter the power goes to a Hewlett Packard (HP) 764D Dual Directional Coupler, rated at 215 to 450 MHz. A diagram of this directional coupler is shown in Figure 2-5a. Power is being fed into port 1. Most of the power comes out at port 2. Power at port 3 is approximately 20 dB down from the power at port 1. Very little power is coming out at port 4. The coupling factor of 20 dB at port 3 is only approximate and varies as a function of frequency. It has been experimentally determined for the different frequencies of interest. Reflected power from further along the transmission line will enter at port 2. Most of the power will come out at port 1. Power out at port 4 is approximately 20 dB down from the power fed into port 2. Again, the exact coupling factor has been experimentally determined for the various frequencies of interest. Therefore, the directional coupler helps in measuring power flow very accurately. Now power need only be measured at ports 3 and 4 to know within the accuracy of the respective coupling factors the power into the Crawford cell and the power reflected from the Crawford Cell. The advantage of this technique is that power measurements can be made while the Crawford Cell is irradiating an

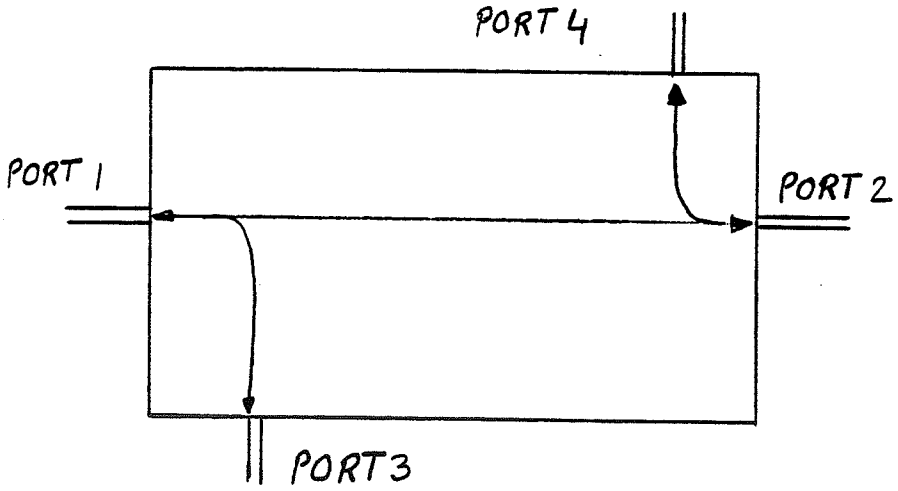

Figure 2-5a. Hewlett Packard Dual Directional Coupler.

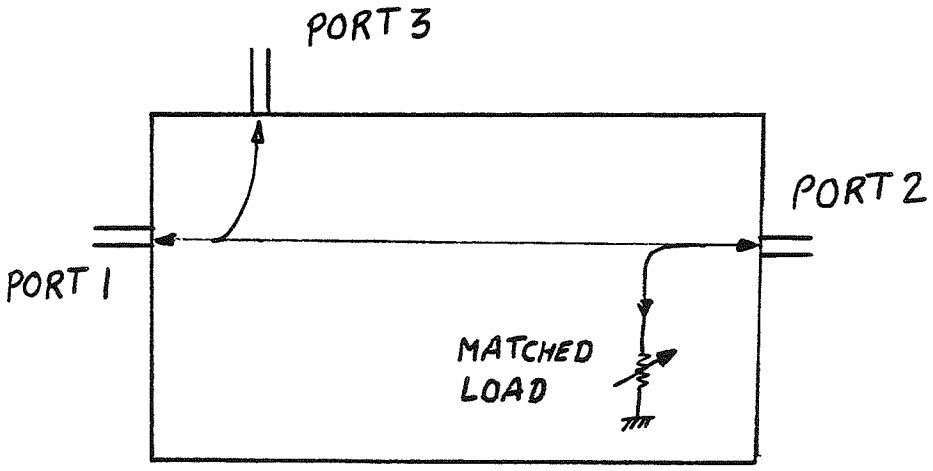

Figure 2-5b. Narda Directional Coupler.

object, without in any way perturbing the fields or the flow of power.

From port 2 of the directional coupler the power goes to the input port of the Crawford Cell. TEM waves will now propagate down the cell. Any object put in the space between the center conductor (septum) and the outer conductor will be irradiated with these TEM waves and dosimetry can be done.

From the output port of the Crawford Cell the power goes to a Narda Coaxial Directional Coupler, rated at 225 to 460 MHz, model # 3000-20. A diagram of this directional coupler is shown in Figure 2-5b. Power out at port 2 is approximately 20 dB down from the power in at port 1. Again, the exact coupling factor has been experimentally determined. By measuring the power at port 3, power transmitted is known accurately. By measuring power into, power reflected and power transmitted from the Crawford Cell, the SARN of the irradiated object can be calculated as will be shown later.

From port 2 of the Narda directional coupler the power goes to a Bird Thermaline Wattmeter Load, model # 824, rated for 5000 W, 50 ohms. This is a water cooled load. It is necessary to have this kind of load because 80 Watt exposures for up to one hour are typically done. A normal 50 ohm load would display all kinds of second order effects for those exposure conditions, which is unsatisfactory.

Power from ports 3 and 4 of the HP directional coupler and port 3 of the Narda directional coupler goes to a 3 way Transco SP3T coaxial RF switch. The output of this switch is monitored by a Hewlett Packard 8481A power sensor. The power measured by the HP power sensor is then displayed on a digitally programmable Hewlett Packard 436A power meter. Since the 20 dB attenuation provided by the directional couplers is not sufficient to keep the power into the SP3T switch from heating it up and causing it to act intermittently, further attenuation was needed. For this purpose, Narda precision attenuators, model # 119A/4, DC to 12.4 GHz were used. The power from port 3 of the HP directional coupler (henceforth called the forward power) is attenuated further by using a 20 dB pad. The power from port 4 of the HP directional coupler (henceforth called the reflected power) is attenuated by attaching a 6 dB pad. Finally, the power from port 3 of the Narda directional coupler (henceforth called the transmitted power) is attenuated by attaching a 10 dB pad. Since these attenuation factors (6,10,20 dB) can change with frequency, they were experimentally determined for the different frequencies of interest.

The frequency of operation of the exposure system was measured by taking a signal from the RF power generator to a DSI frequency counter, model # 5600A, rated from 50 Hz to 512 MHz. This signal was taken from an output terminal on the generator provided exclusively for the purpose of measuring the frequency. Therefore in no way is the power flow into the Crawford Cell being interrupted. (Since the power level at the RF sampling terminal

of the generator saturated the frequency counter, a Microlab 25 dB attenuator, model # FXR AB-25N was used to attenuate the sampling signal to measurable levels.)

Greg Pucci in his Master's thesis (29) provided a computer interface with the Crawford Cell exposure system. The system is now automated to a relatively sophisticated degree and SARN calculations are easy to do. By typing in commands on a Hazeltine CRT screen, control of the switching speed of the SP3T RF switch is possible. The HP power sensor/meter system will now measure forward, reflected and transmitted power levels and send that information to the LSI-11 minicomputer. The different calibration factors ,i.e., the directional coupler coupling factors and the Narda precision attenuation factors, are stored in the minicomputer. A software routine on a floppy disk converts the power levels measured by the programmable HP power meter into actual power levels by multiplying them with their respective calibration factors. The software routine then calculates the power density (P.D.) of the incident electromagnetic field and the specific absorption rate normalized (SARN) of the absorber, as the exposure is taking place by a procedure which will be described a little later. The information is then printed out on the CRT screen for that particular experimental run. It is therefore possible to do RF exposures of prescribed lengths of time, sample the power levels at a specific programmable sampling rate, calculate the SARN and P.D. for that particular experimental run and then take the average of many exposures for the SARN and the P.D. of the object. Statistical analysis of the

data can now be done by doing many exposures, a feature very well suited for dosimetry studies.

B. Theoretical Basis for Exposure

In this section the equations on the basis of which the electromagnetic dosimetry was done will be developed. In general, the electric and magnetic fields for a propagating wave inside the Crawford Cell can be expressed as <exp(jwt) time convention assumed>

$$\bar{E} = \hat{e}\left[E_0 e^{-j\beta x} + \Gamma E_0 e^{+j\beta x}\right]$$

$$\bar{H} = \hat{h}\left[\frac{E_0}{\eta} e^{-j\beta x} - \frac{\Gamma E_0}{\eta} e^{+j\beta x}\right]$$

where

β is the phase constant (= 2 $/\lambda$)

Γ is the reflection coefficient = $|\Gamma| e^{j\theta}$

η is the intrinsic impedance of air = 377 ohms

$\hat{e}$ and $\hat{h}$ are unit vectors in the direction of the electric and magnetic fields respectively.

In particular, because of a TEM mode of excitation

$$\hat{e} = \hat{z} \quad , \quad \hat{h} = \hat{y}$$

Note that both η and β are real numbers, indicating that there is no attenuation of the signal. The power density (P.D.)

is given by

$$\mathrm{Re}\left[\bar{E}\times\bar{H}^{*}\right]\cdot\hat{x}$$

$$= \mathrm{Re}\left[E_0 e^{-j\beta x} + \Gamma E_0 e^{+j\beta x}\right]\left[\frac{E_0}{\eta} e^{+j\beta x} - \frac{\Gamma E_0}{\eta} e^{-j\beta x}\right]$$

$$= \mathrm{Re}\left[\frac{E_0^2}{\eta}\left[1 - |\Gamma| e^{-j\theta} e^{-j2\beta x} + |\Gamma| e^{j\theta} e^{j2\beta x} - |\Gamma|^2\right]\right]$$

$$\therefore \quad P.D. = \frac{E_0^2}{\eta}\left[1-|\Gamma|^2\right]\ \frac{W}{m^2}$$

$$= \frac{E_0^2\left[1-|\Gamma|^2\right]}{3767}\ \frac{mW}{cm*cm}$$

Similarly, the voltage and current at any point on the septum in the Crawford Cell can be written as

$$V(x) = V_0 e^{-j\beta x} + \Gamma V_0 e^{+j\beta x}$$

$$I(x) = Y_0 V_0 e^{-j\beta x} - Y_0 V_0 \Gamma e^{+j\beta x}$$

where Y_0 is the characteristic admittance. In general,

$$\bar{E} = -\nabla V - \frac{\partial \bar{A}}{\partial t}$$

For a parallel plate system

$$\int \frac{\partial \bar{A}}{\partial t}\cdot d\bar{l} = 0$$

$$\therefore \quad |E| = \frac{V}{d}$$

where d is the separation distance between the septum and the outer wall. Therefore, the magnitude of the incident electric field can be expressed in terms of the average power into the Crawford Cell as follows:

$$P_{ave} = Re\left[V(x)\, I(x)^*\right]$$

$$= V_0^2 \left[1 - |\Gamma|^2\right] G_0$$

$$V_0 = \sqrt{\frac{P_{ave} \cdot G_0}{1 - |\Gamma|^2}}$$

$$\therefore \quad E = \frac{1}{d}\sqrt{\frac{P_{ave} \cdot G_0}{1 - |\Gamma|^2}}, \quad \text{where} \quad G_0 = Re[Y_0]$$

and where P_{ave} is the net power into the Crawford Cell. So, knowing forward power minus negative power and G at the frequency of operation, it is possible to calculate the P.D. The software routine presently in operation makes the approximation that the reflection coefficient equals zero. It is recommended that the software be amended to include the reflection coefficient.

Before being able to do any dosimetric studies at all, it is necessary to accurately measure the calibration factors of the directional couplers. This, as explained earlier, allows the measurement of the flow of power without causing any pertubations. Consequently, AF1, AF2 and AF3 will be designated as forward,

reflected and transmitted attenuation factors respectively.

AF1(dB) = 10*log(Power in port 1/Power out of 20 dB attenuator connected to port 3 of the HP directional coupler)

AF2(dB) = 10*log(Power in port 2/Power out of 6 dB attenuator connected to port 4 of the HP directional coupler)

AF3(dB) = 10*log(Power in port 1/Power out of 10 dB attenuator connected to port 3 of the Narda directional coupler)

From the conservation of energy standpoint

Power loss (PLOSS) = (AF1*PF) - (AF2*PR) - (AF3*PT)

where PF,PR and PT are the forward, reflected and transmitted powers (in milliwatts) as measured by the HP436A power meter. (Note that the attenuation factors have to be converted from decibels). The net power in the Crawford Cell is

Power Net (PNET) = (AF1*PF) - (AF2*PR)

and

% LOSS = PLOSS/PNET * 100

Preceding an actual exposure, an empty cell exposure is done. The computer automated system takes 5 values of the

forward, reflected and transmitted powers from the Crawford Cell. It then averages them to obtain a single forward, reflected and transmitted power value. From this it calculates the power loss and the % LOSS due to an empty cell. The minicomputer then prints out the % LOSS as an empty cell loss (ECL). During an actual exposure, this ECL is subtracted from the power absorbed by the object and the empty cell together to give the whole body average power absorption of the absorber. Hence, the power absorbed by the test object is found from the difference of differences.

Power Absorbed (Pabs) = (AF1*PF) - (AF2*PR) - (AF3*PT) -

%LOSS((AF1*PF) - (AF2*PR))

Hence, the average Specific Absorption rate (SAR) is

SAR = Pabs/mass of the absorber (W/kg)

Normalizing to the incident power density

SARN = SAR/P.D. (W/kg/mW/cm*cm)

CHAPTER III

EXPERIMENTAL RESULTS AND DISCUSSION

A. Empty Cell Calibration

The system attenuation factors are listed in Table 3-1. They increase monotonically with frequency, as expected. Also as can be seen in Table 3-1, the attenuation factors are accurate to better than 0.1% in the worst case and 0.01% in the best case. This level of precision is required for SARN calculations to be meaningful. It was noticed during the experiment that the attenuation factors varied somewhat depending upon the input power levels. Power levels of around 20 W gave slightly different attenuation factors than power levels around 90 W. This is because the signal is attenuated approximately 1000 times (in the transmitted power path for example) and therefore the higher power levels will be less susceptible to noise, giving better results. Since the measurements are being done predominantly in the 80-90 W range, this is the power at which the attenuation factors were measured.

The empty cell loss of the Crawford Cell is listed in Table 3-2. One notices two things immediately. First, unlike a parallel plate waveguide system, or even a coaxial transmission line, the power loss does not increase monotonically with frequency. At 425 MHz the ECL is very low, whereas at other

Table 3-1
System Attenuation Factors.
Average Values ± Standard Deviation; N=7.

Frequency(MHz)	AF1(dB)	AF2(dB)	AF3(dB)
400	39.338±.016	25.964±.014	24.397±.012
425	39.385±.002	26.336±.007	30.229±.020
450	40.198±.006	26.740±.013	30.558±.021
475	40.754±.009	27.801±.017	30.800±.019
500	41.743±.011	28.505±.023	31.649±.018
525	42.905±.008	29.607±.014	32.108±.018
550	43.943±.012	31.766±.018	33.248±.015

Table 3-2
Crawford Cell Empty Cell Loss.
Average Value ± Standard Deviation; N = 48.

Frequency (MHz)	ECL(%)
400	18.758±.185
425	2.137±.103
450	10.966±.235
475	13.494±.303
500	12.790±.256

frequencies it is significantly higher. Secondly, the ECL varies slightly from run to run and day to day. Variations in the chamber temperature, humidity and other factors appear to change ECL. The stability of the RF switch and HP power meter is also important because power levels in the milliwatt range are being rapidly switched whereas the input power is on the order of 80-90 W. A change of 0.1 mW (less than 1%) in the value of the power measured by the HP power meter translates into a change of 0.5 W due to the attenuation factors.This is significant when one realizes that the prolate spheroidal models of hamsters to be discussed later absorb in the neighbourhood of 0.7 W. A change of 0.5 W will also change the ECL by a few tenths of a percent. This would account for the variation in ECL seen, even though it was attempted to minimize this by averaging 5 numbers to get the ECL.

It was also noticed that the actual RF exposure should be done exactly or close to the input power levels for the empty cell run. This is because the system loss is taken as a percentage, whereas the actual power loss may not be expressible as a percentage over a large input power range. For example, ECl = 13.85% at an input power level of 85W at 425 MHz.At the same frequency but at an input power level of 15W, ECL = 11.30%. If, however, both empty cell runs and actual runs are done at the same power levels, then this problem is alleviated. This approach, however, assumes that the loss in the Crawford Cell with the absorber in place is approximately the same as the loss in the

Crawford Cell without the absorber. This has been shown by Crawford to be a good first order approximation (30).

B. Phantom Exposure

Before performing RF dosimetry experiments on hamsters, it is necessary to characterize the exposure conditions in the Crawford Cell. It is desired to know how frequency of exposure, orientation, dielectric constant, conductivity and the physical dimensions of the absorber and its position in the Crawford Cell affect the power absorption. For this purpose a prolate spheroidal model (henceforth called the phantom) was used. Figure 3-1 shows the dimensions and the shape of this model. It is hollow and was constructed using plexiglass (ε_r =2.6-j0.0016) (31). The phantom is asymetric in one plane and does not have any sharp edges. This allows the incident electromagnetic field to be perturbed as little as possible. The phantom contains a salt water solution at a concentration of 0.9% (by weight). This increases the phantom absorption over that of pure distilled water, and the phantom is used as a model for the hamster. This is because,as will be seen later, the absorption of the phantom depends on the conductivity of the salt water solution. As the concentration of salt increases in the solution, the conductivity goes up. (32)

There are 3 possible orientations of the long axis of

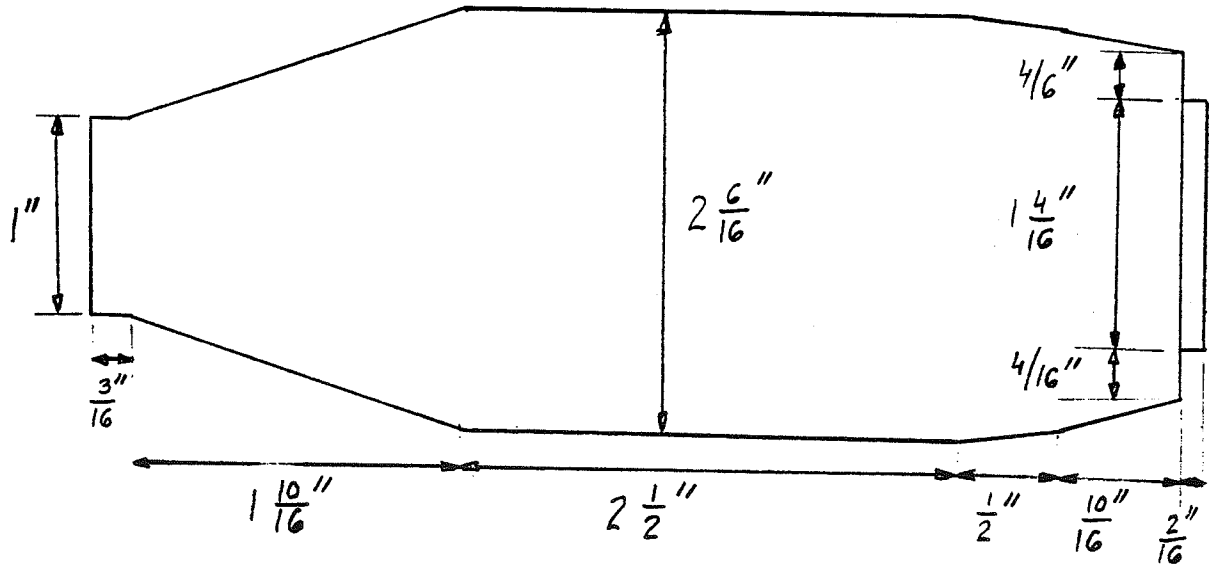

Figure 3-1a. Top View of the Prolate Spheroid Phantom.

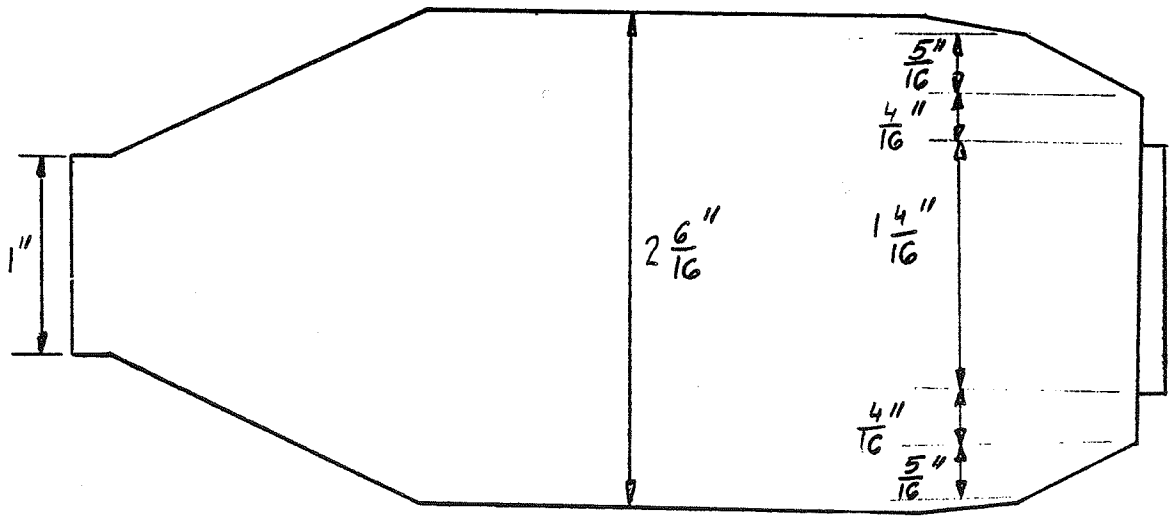

Figure 3-1b. Front View of the Prolate Spheroid Phantom.

the phantom with respect to polarization of the incident TEM waves, namely E, H and K polarizations. In E polarization, the long axis of the phantom is parallel to the E field. In the Crawford Cell that implies that the phantom is perpendicular to the septum. Since the phantom is asymmetric there exist two possible positions. E polarization will imply that the small end of the phantom is facing towards the septum. E' polarization will imply that the small end of the phantom is facing towards the outer wall. As will be shown later,it makes a difference which one of the two orientations the phantom is in. In H polarization, the phantom is perpendicular to the direction of propagation of the TEM wave and parallel to the septum. In this orientation it does not matter what direction the small end of the phantom is pointed. Finally, in K polarization the long axis of the phantom is parallel to the direction of propagation of the energy. Again, in this orientation it does not matter what direction the small end of the phantom is pointed to.

In doing careful RF dosimetry, the repeatability of the experiment is critical. Therefore, for succesive experimental runs the position of the phantom should be exactly the same, to minimize any effect position may have on absorption. In order to investigate this factor two things were done. First, a styrofoam shelf with a relative dielectric constant of 1.03 (31) and of approximately 2.25 cm thickness was used for mechanical support. Based on the power measurements, this styrofoam shelf was seen to be invisible to RF energy. Absolutely no measurable change was detected in the power levels with and without this styrofoam shelf

in the Crawford Cell. The advantage of this shelf is that it allows the phantom to be positioned exactly in the same place for successive runs, if proper care is taken. The second modification of the phantom for experimental purposes was to enclose it in a styrofoam case. This prevents the phantom from rolling along the styrofoam shelf. Again no measurable change in the power levels was noticed with and without this case. Another advantage of this case is that while it is transparent to RF, it can act as a heat insulator. With proper care an exposure of the phantom can be done, and then by placing the phantom in a calorimeter, its total heat content can be measured. By subtracting off the heat content before exposure and assuming that no heat was lost due to leakage through the styrofoam insulation and that all the absorbed energy is converted to heat, the heat content gained (in calories) by the phantom due to just the RF exposre can be calculated. Then by using the following formulas the SARN can be calculated to give an independent verification of the power absorption by the phantom.

X1 (cal)/ 4.186 (cal/J) = X2 (J)

X2(J)/time of exposure(s) = X3 (W)

X3(W)/weight of the absorber (kg) = SAR (W/kg)

SAR (W/kg) / P.D. (mW/cm*cm) =

SARN (W/kg/mW/cm*cm)

It was found that if the exposure duration was kept less than 4 minutes, good agreement between the calorimeter and the Crawford

Cell data were obtained. If however, the exposure duration exceeded approximately 4 minutes, heat insulation became a problem and the calorimeter data became unreliable.

Power absorption measurements were conducted on the empty phantom ,i.e., without any water inside. The weight of the empty phantom is 196 grams. The results of the exposure are shown in Table 3-3. The SARN is a very small number as expected. Its value is just 0.2% of the value the phantom would have had if filled with 9% saline solution. Thus, the absorption of the empty phantom can be neglected. The absorption of the energy is done primarily by the 0.9% saline solution, which weighs 163.6 grams. So from now on, we can consider the phantom to be a 163.6 gram prolate spheroid with 0.9% saline by weight.

SARN measurements on the phantom were done at frequencies from 400 to 500 MHz, in E, E' and H polarizations. The results are shown in Table 3-4. As can be seen, SARN increases as the frequency increases. This is true for all polarizations. This result agrees very well with previous experimental work (24). A typical variation of SARN as a function of frequency taken from the second Dosimetry Handbook is shown in Figure 3-2 and our data are shown in Figure 3-3. Both graphs are remarkably similar. One notices that the SARN increases as a function of frequency until the long axis of the absorber is between 0.36 to 0.40 . For the phantom, the long axis equals 0.1482 m. Therefore, the resonance frequency of the absorber can be calculated as follows:

Table 3-3
SARN for the 163.6 Gram Empty Phantom.
500 MHz, E Polarization. 30 Samples per Data Point.

ECL(%)	SARN(W/kg/mW/cm*cm)	P.D.(mW/cm*cm)
12.52	0.02166	33.964
12.92	0.00101	35.608
12.88	0.01388	38.236
13.23	-0.00307	41.368
13.11	0.01213	40.376

Average = 0.00894

Standard Deviation = 0.0102

Table 3-4
SARN (W/kg/mW/cm*cm) as a Function of Frequency.
163.6 Gram Prolate Spheroid Phantom.
30 Samples per Exposure.
Average Value± Standard Deviation; N = 16.
Incident Power Density Varies From a Minimum of
32.696 (mW/cm*cm). to a Maximum of 58.663 (mW/cm*cm).

	Polarization		
Frequency (MHz)	E	E'	H
400	0.26921±.0056	0.28299±.0069	0.05703±.0085
425	0.41341±.0078	0.43058±.0076	0.08287±.0065
450	0.58408±.0123	0.58995±.0089	0.11040±.0121
475	1.39963±.0288	1.44594±.0140	0.11770±.0165
500	4.86181±.0439	4.94875±.0360	0.13557±.0120

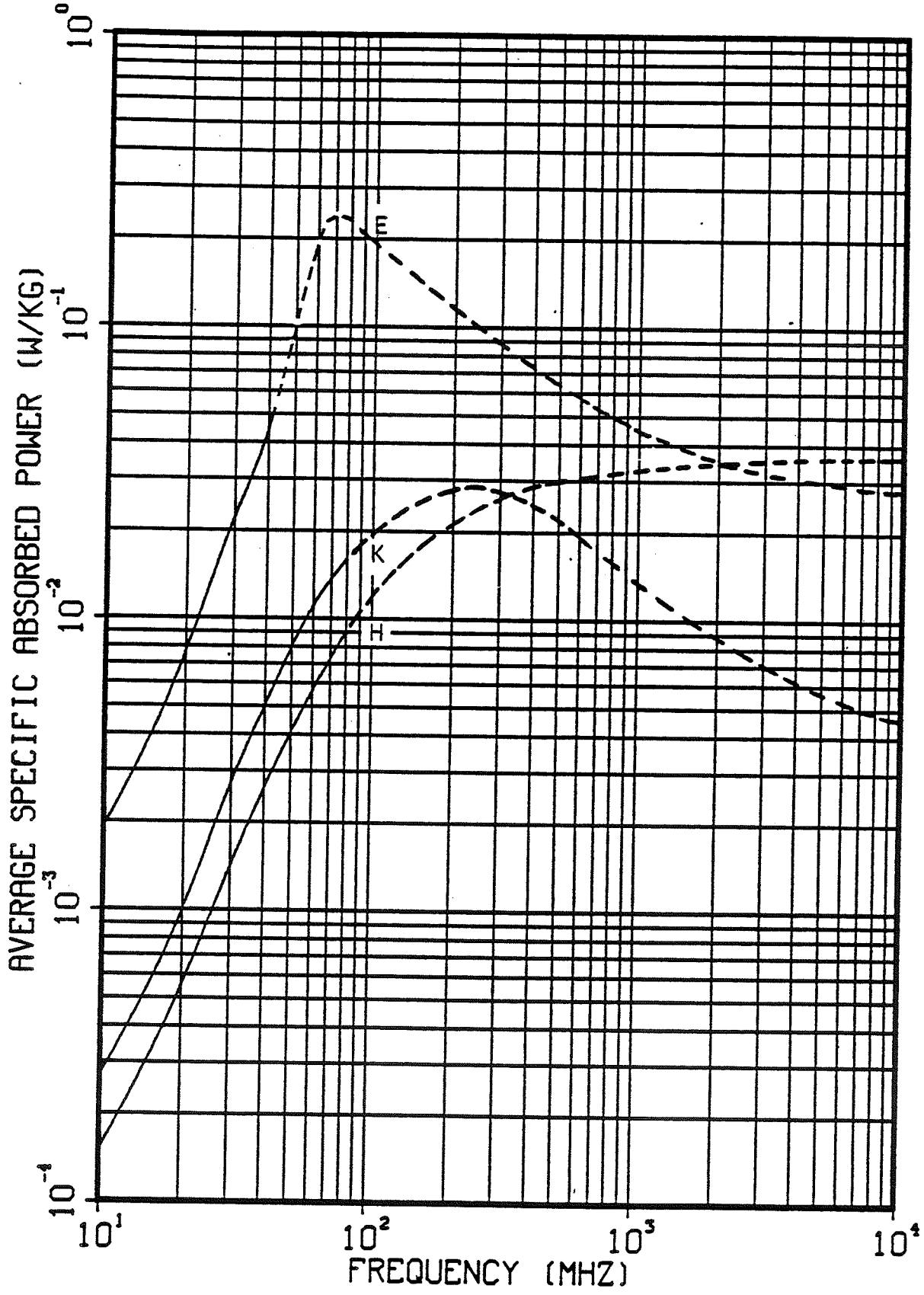

Figure 3-2. SAR as a Function of Frequency for a Prolate Spheroidal Model of Man [24].

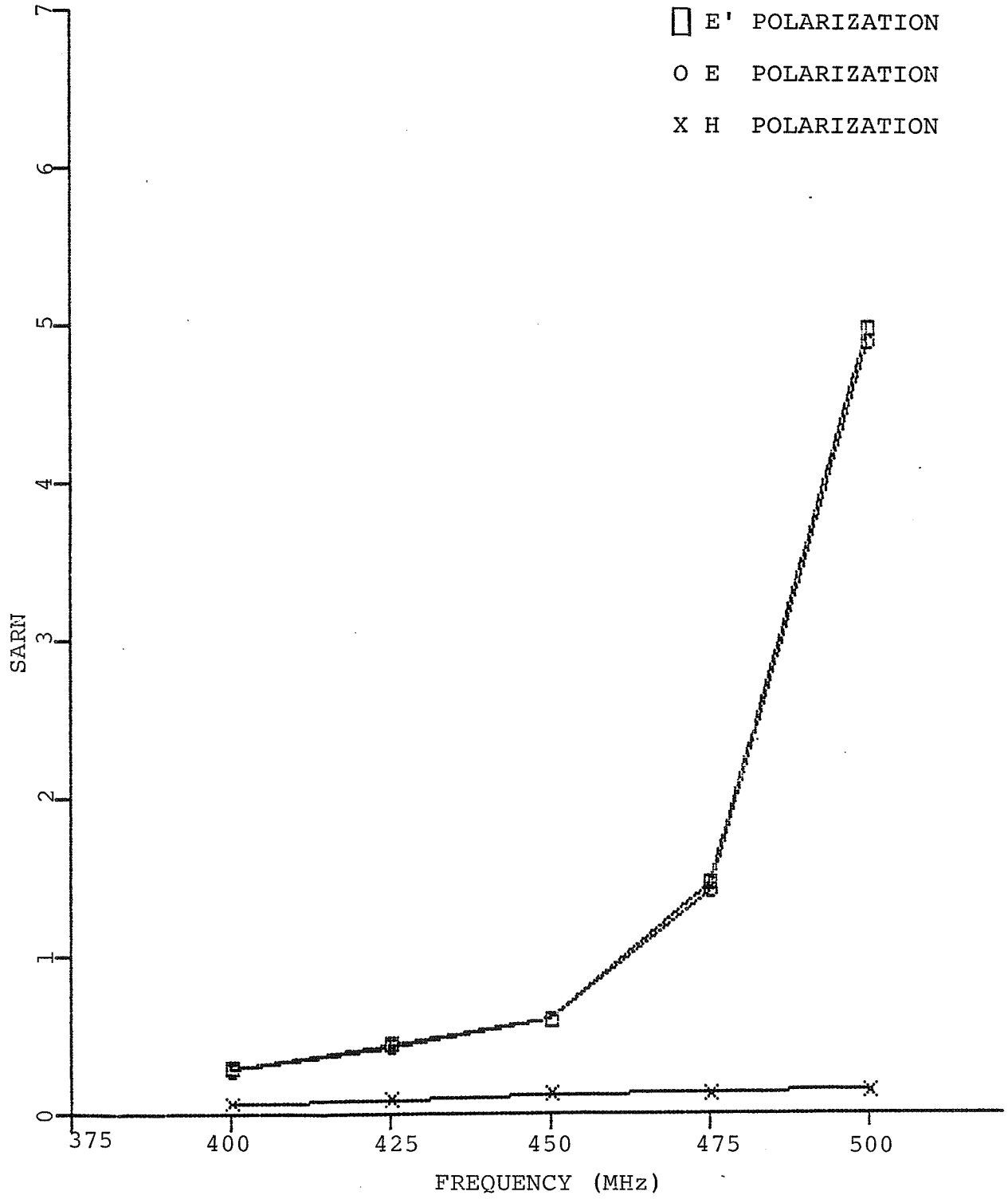

Figure 3-3. SARN (W/kg/mW/cm x cm) as a Function of Frequency.

$$0.4\lambda = 0.1482\,m$$

$$\therefore \lambda = 0.3705\,m$$

$$\lambda \cdot f = c$$

$$\therefore f = \frac{3\times10^{8}}{0.3705} \cong 800\ MHz$$

Since all the exposures were done from 400 MHz to 500 MHz, the absorption is in the pre-resonance range. In this region of the frequency spectrum the SARN exhibits a $f^{2.75}$ to $f^{3.00}$ type of behaviour, as experimentally verified by Gandhi (14). As frequency increases past the resonance point, the absorption goes down, because at high frequencies the conductivity of the absorber becomes so large that the incident electric field is rapidly attenuated. The depth of penetration becomes small and most of the significant field is confined to a small area around the surface. This is the skin depth effect. At one skin depth, the power available in the electromagnetic wave has decreased to 13.5% of the value on the surface. A rough idea of the RF field penetration can be obtained from a plane wave's penetration depth in an infinite dielectric slab (24). There the skin depth in meters is

$$\delta = \frac{67.52}{f}\left[\sqrt{(\varepsilon')^2 + (\varepsilon'')^2} - \varepsilon'\right]^{-1/2}$$

where f is frequency in Megahertz and

ε' is the real part of the relative dielectric constant and

ε'' is the imaginary part of the relative dielectric constant.

For 0.9% salt water (31)

$$\varepsilon' = 76$$

$$\varepsilon'' = 0.78\varepsilon'$$

Therefore at 400 MHz, skin depth equals 37.39 mm. Power is absorbed by only the surface region and, consequently, the whole body absorption goes down. This effect becomes more pronounced as the frequency increases.

For biological media ($\mu_r = 1.0$), the time averaged power absorbed per unit volume P is

$$P = \frac{1}{2}\bar{E}\cdot\bar{J} = \frac{1}{2}\bar{E}\cdot\sigma\bar{E}$$

$$\sigma = \omega\varepsilon_0\varepsilon''$$

$$\therefore P = \frac{1}{2}\omega\varepsilon_0\varepsilon''|E|^2$$

The time averaged power absorbed, normalized to the density of the media is the specific absorption rate (SAR). SAR in terms of the magnitude of the incident electric field is then

$$SAR = \frac{1}{2m/v}\omega\varepsilon_0\varepsilon''|E|^2$$

The whole body absorption is found by integration over the absorber surface. SARN is the power density normalized absorption at a point. The equations for SARN in terms of E and J can be used to explain the data.First, one notices that as frequency increases, conductivity increases ($\sigma = \omega\varepsilon_0\varepsilon''$). The power absorption will then continue to increase in the

pre-resonance region. Beyond the resonance region, the magnitude of the electric field inside the object decreases, due to the skin depth effect as explained earlier. So, in the post resonance region although the conductivity has increased, E is now only significant along the surface. E.J is now nonzero over a smaller volume and thus absorbed power gets smalller. The decreasing size of the region where E.J is significant dominates over the increasing conductivity and whole body SAR falls. This is to be expected, for in the limit the frequency goes to the visible range the absorption goes to zero.

In addition, it can now be explained why E polarization gives a higher absorption than H polarization. At low frequencies,i.e., below resonance, the electric and magnetic fields are approximately independent of each other. Such fields are called quasi static fields. The incident electric field on the absorber induces an electric field E_e inside the absorber body. The tangential component of E_e is continuous across the boundary. The normal component of E_e is dependent upon the permittivity of the absorber. So if the long axis of the absorber is normal to the incident electric field, the tangential component of E_e, which is continous across the boundary ,will be over a small region. The normal component of the electric field in the absorber E_{en}, in terms of the normal component of the electric field incident on the absorber, is then,

$$E_{en} = \frac{\varepsilon_1}{\varepsilon_2} E_{n1}$$

where E_{n1} is the normal component of the incident electric field.

E_{en} is small because $\varepsilon_1 << \varepsilon_2$. Thus the coupling is weak. On the other hand, if the long axis of the absorber is parallel to the incident electric field, the tangential component of E_e will be over a large region and the normal component of E_e will be over a small region. Thus, the coupling is strong. The incident magnetic field also induces an electric field E_h inside the absorber body. E_h circulates about H, corresponding to eddy currents induced by magnets. When the cross section of the absorber body perpendicular to H is large, E_h will be large because a large magnetic flux is intercepted by the body. This results in strong magnetic coupling. When the cross section of the body perpendicular to H is small, E_h will be small. This is a weak magnetic coupling.

Therefore, in E polarization both electric and magnetic field couplings are strong because the longest axis of the absorber is parallel to the electric field and the cross sectional area normal to H is large. In H polarization both couplings are weak because the axis parallel to the electric field is small and the cross sectional area normal to H is also small. Finally, in K polarization the electric coupling is weak and the magnetic coupling is strong.The total power absorbed is proportional to $(E_e + E_h)^{**2}$. Therefore, for frequencies below resonance, most power will be absorbed in E polarization, the least with H polarization, and a value in between for K polarization.

Finally, (although this is difficult to see from

Figure 3-3, it is clear in Table 3-3) it can now be explained why E' polarization gives a slightly higher absorption than E polarization. If the incident electric field were uniform, the E,E' polarizations would be equivalent. But, from measurements it is known that this is not true. Ideally, the electric field distribution inside the Crawford Cell when the phantom is being irradiated should be mapped. This, however, was not possible due to the unavailabilty of a good electric field probe. So, the following experiment was done. SARN as a function of position was measured at 1 cm intervals in the E,H and K planes. The data were obtained at 475 MHz for the phantom in H polarization. This data are plotted in Figures 3-4 through Figures 3-6. As can be readily seen from Figure 3-4 the SARN is maximum when the phantom is next to the septum and minimum when placed against the outer wall. This can be explained if the incident electric field varied in the E plane, with a maximum at the septum and a minimum at the outer wall. When the phantom is in E polarization, the small end is pointing towards the septum (and the large end is pointing towards the outer wall). The region containing the small end has the strongest electric field. In the E' polarization, the region containing the large end is in the strongest electric field, with a variation down the axis of the phantom. Naturally, then it is expected for the E' polarization to have a slightly higher SARN, in light of the E.J behaviour of the power absorbed.

As can be seen from Figures 3-5 and 3-6, the SARN is not a strong function of position in the H and K planes as long as the absorber stays away from the extremities of the Crawford Cell.

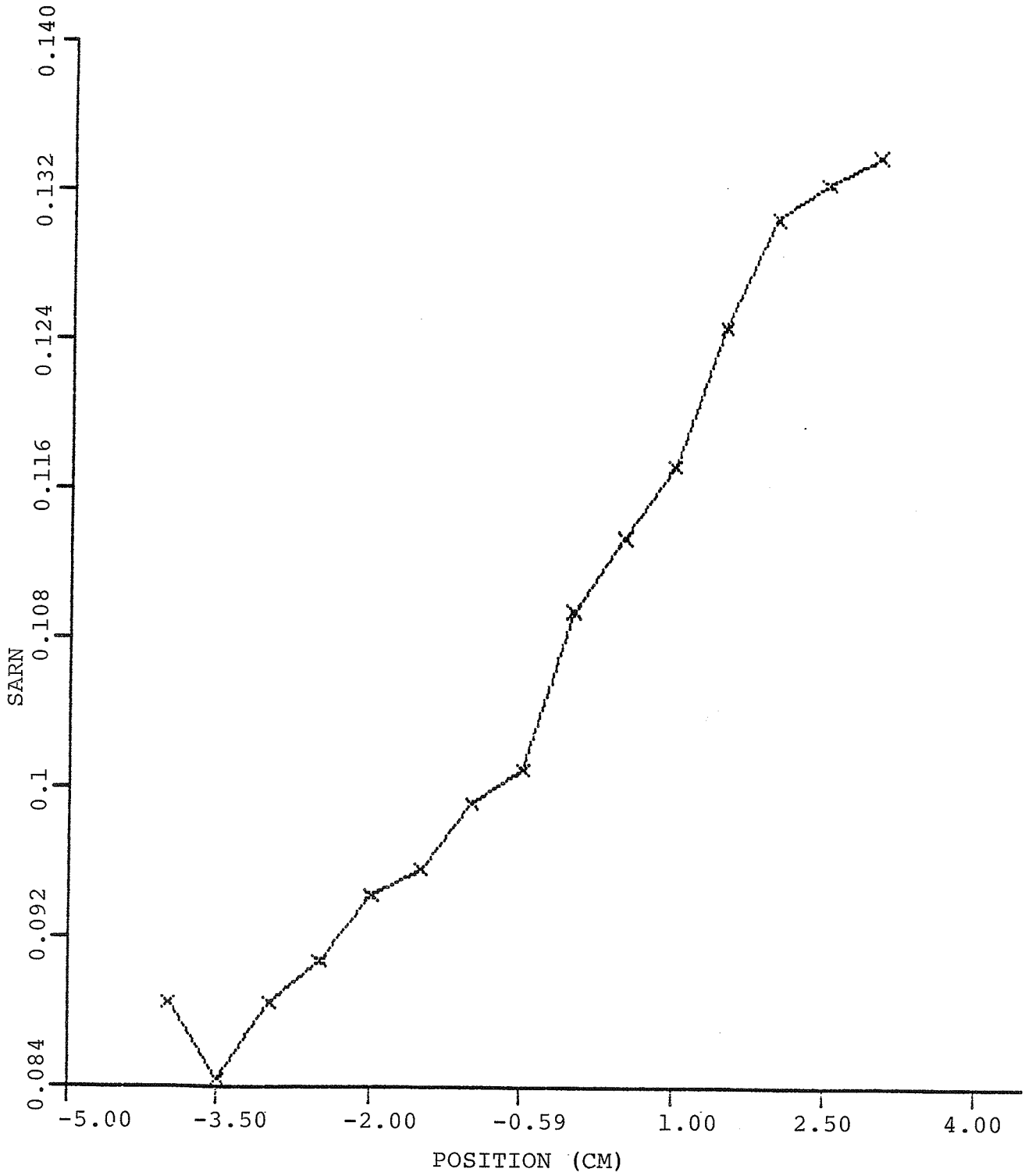

Figure 3-4. Variation of SARN(W/kg/mW/cm x cm) in the E Plane.

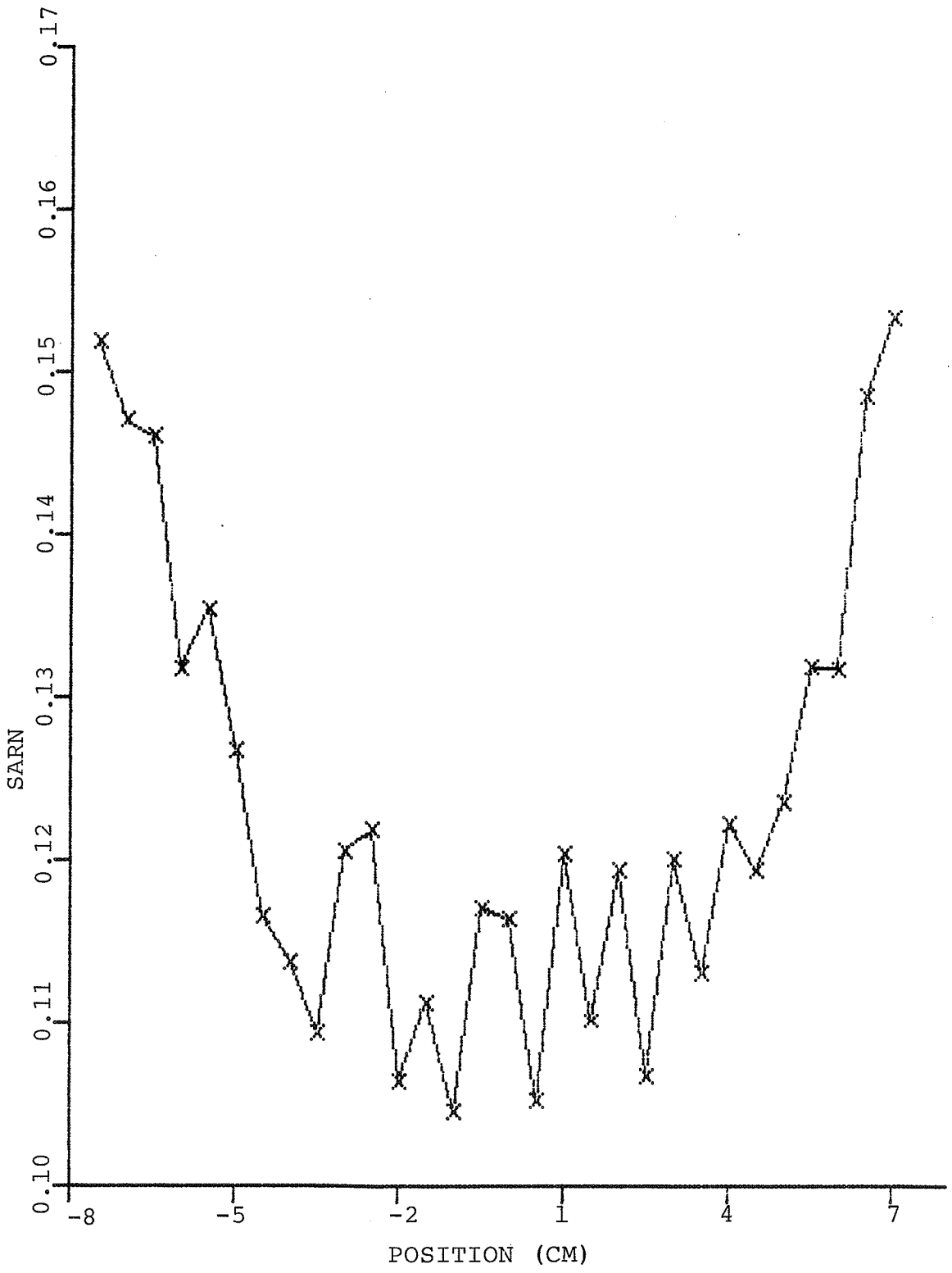

Figure 3-5. Variation of SARN(W/kg/mW.cm x cm) in the H Plane.

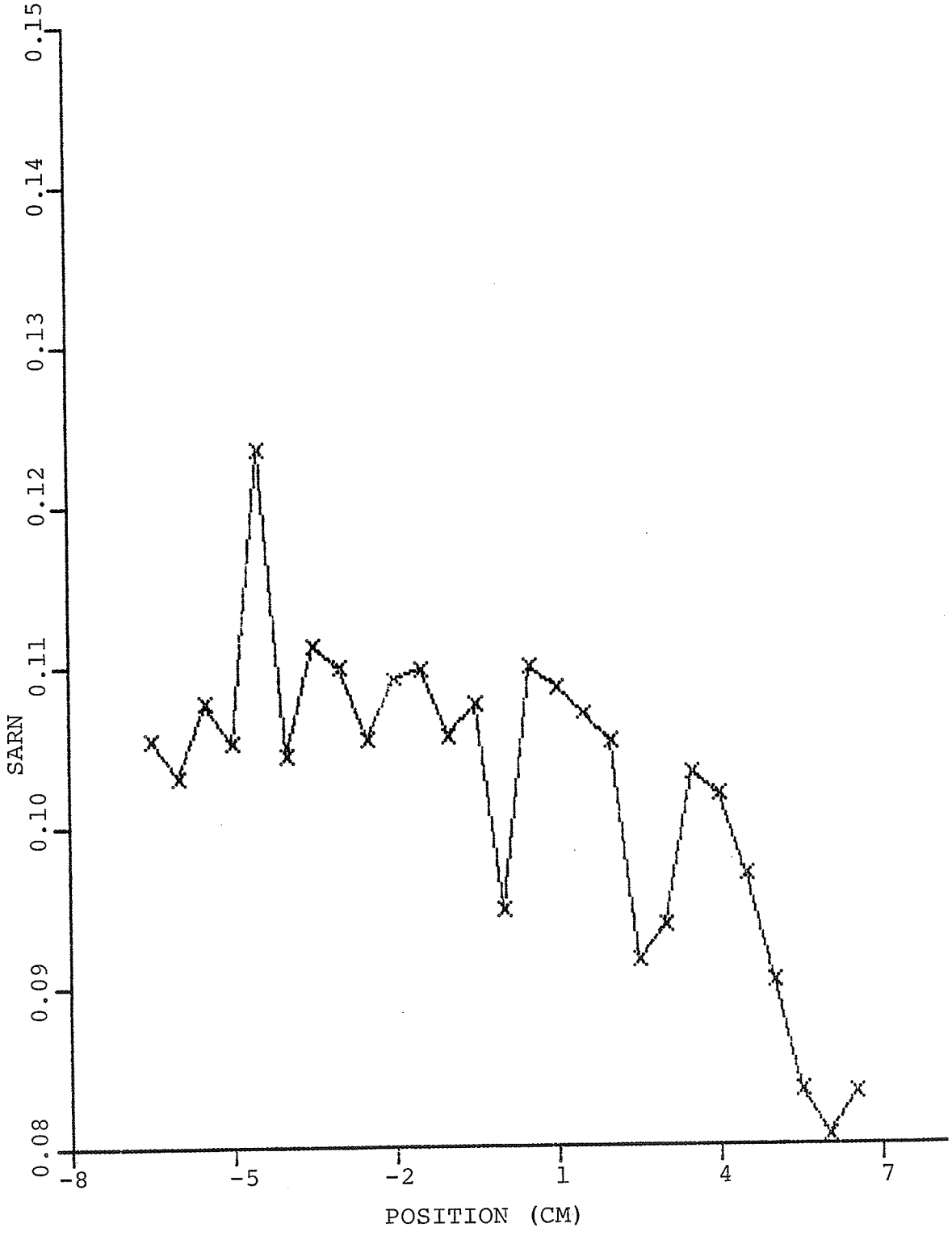

Figure 3-6. Variation of SARN(W/kg/mW/cm x cm) in the K Plane.

In the H plane as the absorber gets close to the front or back wall, the gap between the septum and the outer wall becomes small (2.5 cm as seen from Fig.2-2). Therefore, the electric field intensity is greatest here and the SARN is expected to increase. In the K plane SARN is uniform if one allows some variations in the data. It is only when the phantom is positioned close to the output port of the Crawford Cell does the SARN tend to decrease.

In Figures 3-4 to 3-6, the position equal to 0 indicates the position where the SARN data were taken for Table 3-4. It is located approximately in the center of the Crawford Cell. When placing the phantom in the same position for successive absorption measurements, the position in the H and K plane is not critical. If, however, care is not taken and the phantom is not in the exact same position in the E plane, the SARN will subsequently change. It will increase if the phantom is moved closer to the septum and decrease if moved away. In Figure 3-4, a position greater than 0 indicates movement towards the septum. In Figure 3-5, a position less than 0 indicates movement towards the back door. Finally, in Figure 3-6, a position greater than 0 indicates movement towards the input port of the Crawford Cell. Since in each of these positions the SARN of the phantom is being measured in E,H and K polarizations only, it is important that the phantom have an angle of 0 degrees with respect to the horizontal. This avoids any intermediate polarizations with correspondingly intermediate SARN's.

Finally, since dosimetry experiments on hamsters for

extended periods of time are planned for the future, the variation of SARN as a function of time was also determined. Results are plotted in Figure 3-7. One notices a linear variation with time, because as the phantom absorbs the RF energy it heats up. The conductivity of water increases as the temperature increases (32). Since the SAR is directly proportional to conductivity, the linear increase in absorption is seen. Since the SARN plotted in Figure 3-7 is an averaged SARN over the length of the exposure, the actual SARN at say, 45 minutes, is much higher than the one shown in the figure.

C. Hamster Exposure

In the second phase of this project, the absorption of Syrian hamsters is studied. Because of the SARN variability with position, it is important that the hamster have approximately the same position each time. Cylindrical plexiglass cages were constructed for this purpose. The radius of the circular aperture is 6.3 cm and the length of the cylinder is 13.9 cm. These dimensions were chosen because anything longer would not fit in the Crawford Cell and anything shorter would not be long enough for the hamsters. The cages are wide enough for the hamsters to be able to turn around. It is expected that the absorption of these cages to be minimal because they contain very few sharp edges and they are made from plexiglass. From experiments, this was confirmed.

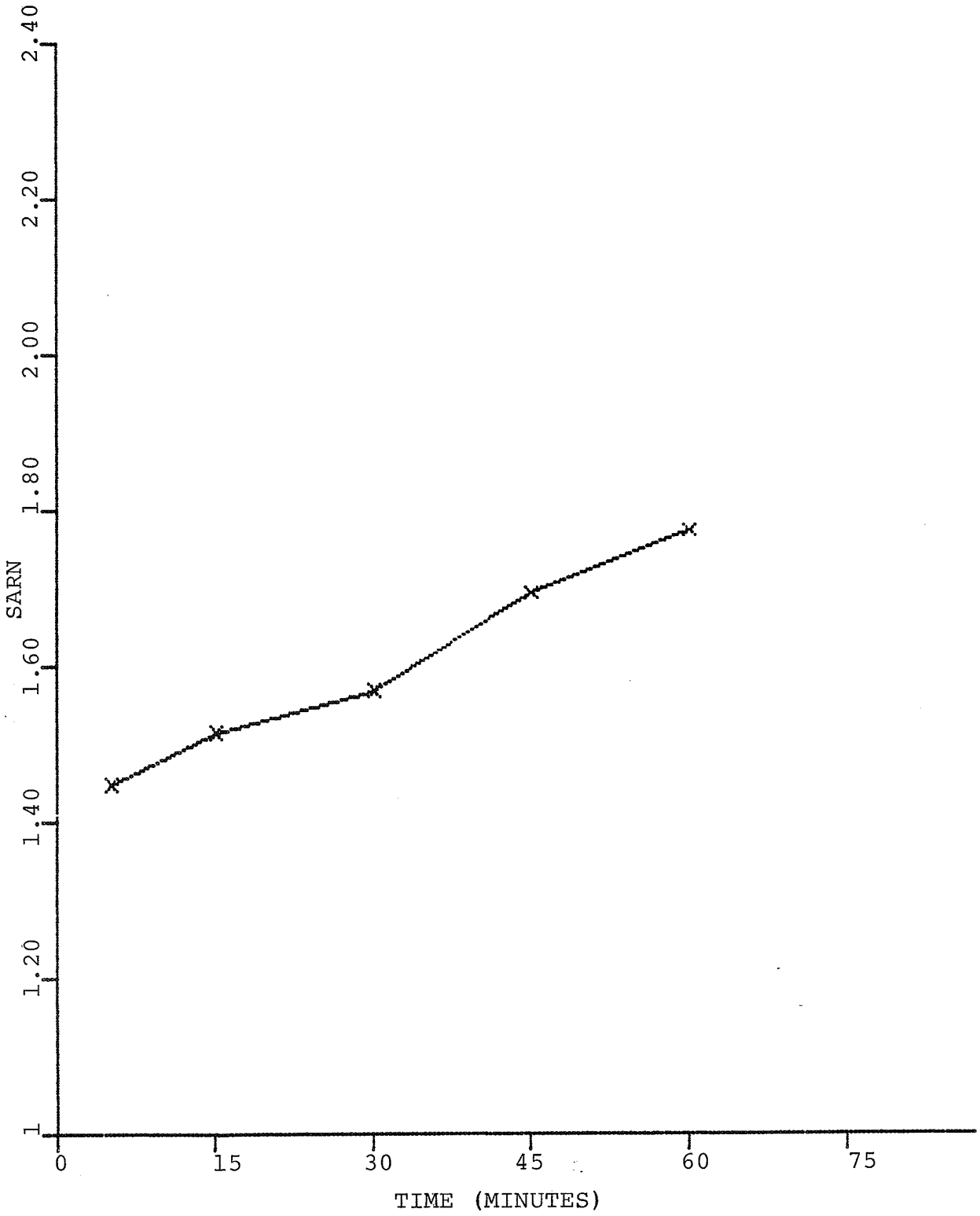

Figure 3-7. SARN(W/kg/mW/cm x cm) as a Function of Time.

The RF energy can affect the hamster by raising its body temperature. The rectal temperatures of the hamsters were measured by using a YSI Tele-thermometer with a LN0297 model#402 probe . On the probe, 4 cm was marked off so that in each hamster the probe recorded the temperature of roughly the same tissue area. Prior to exposure, it was found necessary to train the hamsters to accept the process of measuring their rectal temperatures without becoming too excited. Excited hamsters showed a temperature rise of approximately 2°C above resting animals. Untrained hamsters would get excited and defecate extensively, making temperature measurements after exposure useless. In approximately one week, it was possible to get the hamsters accustomed to having their rectal temperatures measured.

Initially, the effects of confining the hamsters to the plexiglass cages were a matter of concern. It were thought that restraining the hamsters would get them excited, thereby raising their temperatures. Actually, the exact opposite was seen to happen. After an initial period of 15 minutes in which they moved about the cage, the hamsters fell asleep. The rectal temperature of a hamster that was asleep is approximately 36.5 °C. Therefore, any rise in rectal temperature is due entirely to the RF exposure.

Some dosimetry data on 15 cm Syrian hamsters are shown in Figure 3-8. This data were obtained from 2 hamsters. On a particular day, one hamster was exposed to RF and the other was kept as a sham. On the next day, the RF exposed hamster became

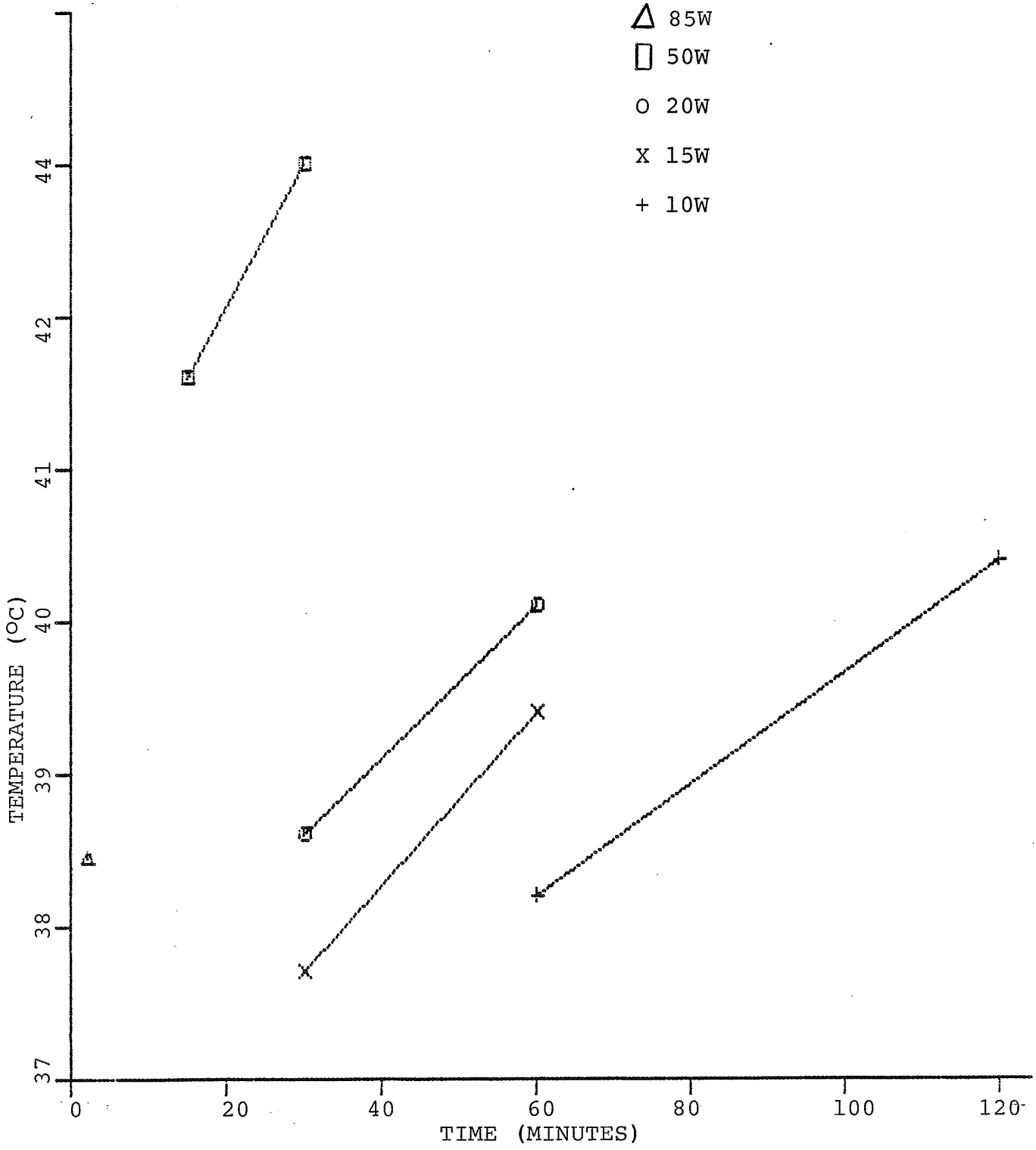

Figure 3-8. Temperature Rise of 15cm Syrian Hamsters as a Function of Time of Exposure and Input Power in E Polarization.

the sham and the sham hamster became the RF exposed hamster. This pattern was repeated until all the data were obtained. A temperature of 43 ^{o}C was seen to kill the hamster.As their temperatures increased, the hamsters extensively salivated, their skin became wrinkled and they defecated. Increasing the incident power density or increasing the length of exposure led to increased absorption . An input power level of less than 8 W did not raise the hamster's rectal temperature. On the other hand, an input power level of 80 W for just 2 minutes was sufficient to raise the hamster's rectal temperature to 38.5^{o}C.

It was seen that the power absorption is a very strong function of the length of the hamster (E.J dependence of SARN). An attempt was made to repeat the dosimetry data of Figure 3-8, using smaller hamsters (approximately 10 cm in length). Although less absorption due to a shorter length was expected, it was thought that hamster rectal temperatures would rise by approximately the same amount due to a smaller volume of tissue. This was found to be incorrect. It was found that an input power level of 40 W for up to one hour of exposure produced no measurable change in the rectal temperatures of the hamsters. This is in sharp contrast to the results shown in Figure 3-8. This is explained by the shorter lengths and the significant fact that the hamsters tended to curl up into little balls. This made their effective lengths even smaller. It required an input power level of 80 W for an exposure duration of 30 minutes to get the hamster temperature into the 39 - 40 degree celsius range. For the 10 cm (4 inch) hamsters, then, the dosimetry curves look very

similiar to those in Figure 3-8, except that the input power levels are shifted up.

The experiments up to this point were performed without considering the problem of unequal loading of the two chambers of the Crawford Cell. In all the phantom exposures, one chamber would contain the phantom and the other chamber would be empty. However, it was desired to expose two hamsters simultaneously. This would allow a check on both the hamster rectal temperature measurements and the biological assay experiments. Here, the effects of unequal loading of the two chambers were noticed. Some typical data are shown in Table 3-5. The data must be considered in groups of two. The SARN value is for both the hamsters taken as one absorber. At low input power levels, no measurable change is seen in the hamster temperatures. However, at high input power levels noticeable effects are seen. SARN is the absorption rate normalized to the incident power density and the density of the absorber. So, if two hamsters are exposed to the same SARN levels, their temperatures should rise about the same. However, this is not seen if the two hamster weights are different. In all the exposure cases, the heavier hamster absorbs much more. It is possible to put two hamsters in the two chambers with a weight difference of only 4 grams (approximately 4% of body weight) and still see a temperature differential of up to 4^{o}C.

The reason for this is that the two chambers are coupled and can be modelled as parallel loads on a transmission

Table 3-5
SARN for the 10 Cm Syrian Hamster.
475 MHz, E Polarization. 10 Second Sampling Rate.
Hamster Weight is in Grams. Power in is in Watts.
Time of Exposure is in Minutes.
Units of SARN are W/kg/mW/cm*cm. Units of P.D. are mW/cm*cm.
Temperature is in Degrees Celsius.

Hamster Wt.	Power In	Time	SARN	P.D.	Temp.
78	20	60	0.10185	9.933	37.4
80	20	60	0.10185	9.933	36.0
81	40	60	0.12323	20.139	36.4
79	40	60	0.12323	20.139	36.8
96	60	60	0.20818	30.760	37.0
100	60	60	0.20818	30.760	39.3
98	70	60	0.25677	35.270	40.2
94	70	60	0.25677	35.270	39.4
114	80	30	0.28400	40.297	40.8
100	80	30	0.28400	40.297	38.0
100	80	30	0.25017	40.369	40.8
98	80	30	0.25017	40.369	39.7
101	80	30	0.21124	40.210	40.0
100	80	30	0.21124	40.210	38.9
101	80	30	0.16236	42.157	39.1
100	80	30	0.16236	42.157	37.8
104	80	30	0.33650	41.744	39.0
112	80	30	0.33650	41.744	42.3

line. The equivalent cicuit model is shown in Figure 3-9. In that figure, Z1 represents the impedance presented by hamster#1, and Z2 represents the impedance presented by hamster#2.

For dielectric materials, the wave impedance is

$$Z = \sqrt{\frac{u}{\varepsilon}} = \sqrt{\frac{u}{\varepsilon_0(\varepsilon' - j\varepsilon'')}} \quad , \quad \varepsilon'' = \frac{\sigma}{\omega\varepsilon_0}$$

$$\therefore Z = \sqrt{\frac{u}{\varepsilon_0\sqrt{(\varepsilon')^2 + (\varepsilon'')^2}\, e^{j\tan^{-1}(-\varepsilon''/\varepsilon')}}}$$

For 0.9% salt water (31),

σ = 15.2 mmhos/cm

ε' = 76

$$\tan\delta = \frac{\varepsilon''}{\varepsilon'} = 7800 \times 10^{-4}$$

$$\therefore \varepsilon'' = 0.78\varepsilon'$$

$$\therefore Z = \sqrt{\frac{u}{\varepsilon_0\left((76)^2 + (59.28)^2\right)^{1/2} e^{j\tan^{-1} 0.78}}}$$

$$\therefore \mathrm{Re}[Z] << 377\,\Omega$$

The bigger the hamster, over more space the dielectric material exists, the smaller the equivalent impedance. Therefore, the heavier hamster impedance Z1 is less than the lighter hamster impedance Z2.

Power absorbed by Z1 = $V^2/\mathrm{Re}[z1]$

Power absorbed by Z2 = $V^2/\mathrm{Re}[z2]$.

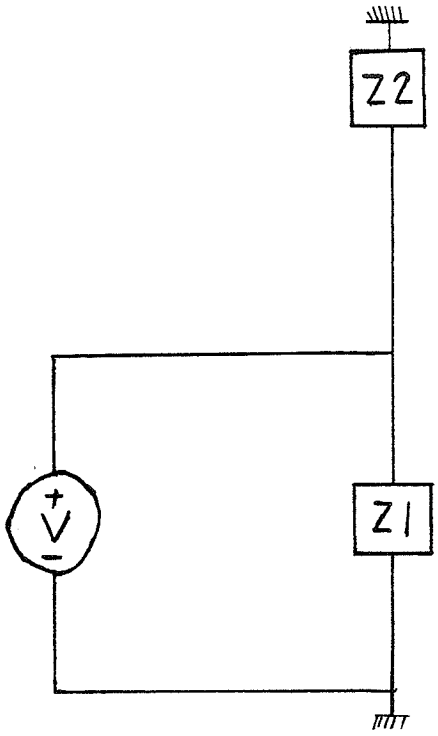

Figure 3-9. Equivalent Circuit Model for Loading the Two Chambers of the Crawford Cell.

Because the real part of Z1 is less than the real part of Z2, the heavier hamster will absorb more energy.

Finally, it was desired to see if the absorption varied from day to day. Some data are presented in Table 3-6. Once again the data must be considered in groups of two. There is a little variation, but not much. One has to realize that the plexiglass cages give the hamsters room for movement. So, on any given day, although the plexiglass cage might be in the exact same position, the hamster may not. As explained earlier, SARN is a very strong function of position. If theoretically one were to consider the hamster curled up in a ball at the two extremities of the cage, different absorptions would occur. Not only does the hamster position affect its absorption, it also affects the absorption of the adjoint hamster, because of coupling between the chambers. One way to reduce this problem is to build smaller cages. Actually, there may be a way around this problem. This is because we noticed a very interesting phenomena in the hamster exposure. In 99% of all cases where the hamster absorbed enough energy to be distressed, it was noticed that the hamster orientated itself with its head pointing towards the septum. This is the region of the strongest electric field. This is surprising when one realizes that the hamster could curl up in a ball at the other end of the cage,i.e., where the electric field is weaker.

Table 3-6
Day to Day Variations in SARN for 10 Cm Hamsters.
475 MHz, E Polarization. 30 Samples per Data Point.
Hamster Weight is in Grams. Time of Exposure is in Minutes.
Units of SARN are W/kg/mW/cm*cm.
Units of P.D. are mW/cm*cm.Temoerature is in Degrees Celsius.

No.	Hamster Wt.	Power In	Time	SARN	P.D.	Temp.
1	99	80	30	0.29212	40.296	40.4
2	98	80	30	0.29212	40.296	40.5
3	104	80	30	0.23038	40.267	39.2
4	104	80	30	0.23038	40.267	39.5
5	112	80	30	0.32711	40.142	40.5
6	112	80	30	0.32711	40.142	41.7
3	104	80	30	0.29759	40.340	40.2
4	104	80	30	0.29759	40.340	39.3
1	99	80	30	0.33166	41.908	39.8
2	98	80	30	0.33166	41.908	40.5
5	112	80	30	0.35919	42.350	40.5
6	112	80	30	0.35919	42.350	42.5

CHAPTER IV

CONCLUSION

In this thesis the absorption characteristics of a 0.9% saline filled prolate spheroid have been presented. The effects of absorber geometry, position and conductivity, frequency of operation and loading of the Crawford Cell on the absorption have been shown. The power absorption increases with conductivity, length of the test object in wavelengths and frequency of operation. The absorption versus frequency curve shows a sharp resonance when the longest axis of the test object is in E polarization and approximately 0.4 wavelength in length. Beyond resonance, the absorption decreases. The absorption is strongest in E polarization, weakest in H polarization and intermediate in K polarization. The absorption is not sensitive to small variations of the test object in the H and K planes, but very sensitive to variations in the E plane. It has been experimentally determined that there is a variation of the electric field in the E plane . The electric field is strongest at the septum and weakest at the outer wall. It has also been shown that if the Crawford Cell is unequally loaded, the power absorption is also unequal among the two test objects. Finally, it appears that the SARN is the same for different incident power levels,i.e., absorption is linear with respect to power density levels. It is hoped that SARN (as opposed to SAR) becomes the future common denominator for reporting dosimetry results.

Some dosimetry on hamsters has also been done. Any radio frequency energy absorbed is converted to heat which causes the rectal temperature of the hamster to rise. A temperature of 43 ^{o}C was found to be high enough to kill the hamster. However, the absorbed power is a very strong function of length and weight of the hamster. Therefore, an exposure condition which causes a certain temperature rise in one particular hamster will not cause the same temperature rise in another similiar hamster.

CHAPTER V

RECOMMENDATIONS

It was observed that the MGL power generator is sensitive to its load,i.e., the Crawford Cell. Changing the object to be irradiated, or its position, changes the impedance of the Crawford Cell. This adversely affects the power generator and causes the frequency and amplitude to drift. It is recommended that an RF isolator be installed at the output port of the power generator. It is also recommended that an RF isolator be installed at the load. As can be seen from the Appendix, the load is not a perfect 50 ohm match over the frequency range of interest. Some reflections may be getting back into the Crawford Cell. This reflected power is irradiating the absorber, thus causing the absorption to be greater than it should be. An RF isolator at the load will alleviate this problem.

Although not reported in this thesis, initially some dosimetry in the 225 to 300 MHz region on prolate spheroid models, using a different power generator, was done. The prolate spheroid absorbs power on the order of 0.6 - 1.0 W when the input power level is on the order of 80 - 90 W. The empty cell loss is on the order of 6 - 8 W. The same order of magnitude holds for higher frequencies as well. Therefore, an accuracy of greater than 1.0% is required. An error of 0.5 W in the empty cell loss computation would be catastrophic for calculating the SARN. This shows the

paradoxical result that it is easier to accurately determine the power absorbed by the test object than the power absorbed by the empty cell, even though the latter is an order of magnitude greater. It is therefore important that the system have as little loss as possible and be calibrated accurately. Cables should be as short as possible. It is recommended that attenuators be used that do not vary significantly with time. Finally, no matter how carefully the system is set up, the SARN can still vary substantially if the frequency of operation is low, the input power level is low or the size of the absorber is small. Therefore, some kind of averaging over extended periods of time may be necessary. For this purpose, computer automation is ideal.

Much more needs to be done before RF dosimetry is fully understood or clinical hyperthermia is possible. Extensive biological assays need to be done on the non-thermal effects of non-ionizing radiation. Because increasing size means increasing the absorption substantially, dosimetry experiments have to be done on larger animals than hamsters before applying analogies for human exposure conditions. Also, the state of the art for focusing electromagnetic radiation is not advanced enough to provide the focusing capabilities required for near field exposures of humans. So it is hoped that funds are available in the future to continue research activities in this area.

APPENDIX

COMPONENT FREQUENCY RESPONSES AND ABSORPTION CHARACTERISTICS OF THE PHANTOM

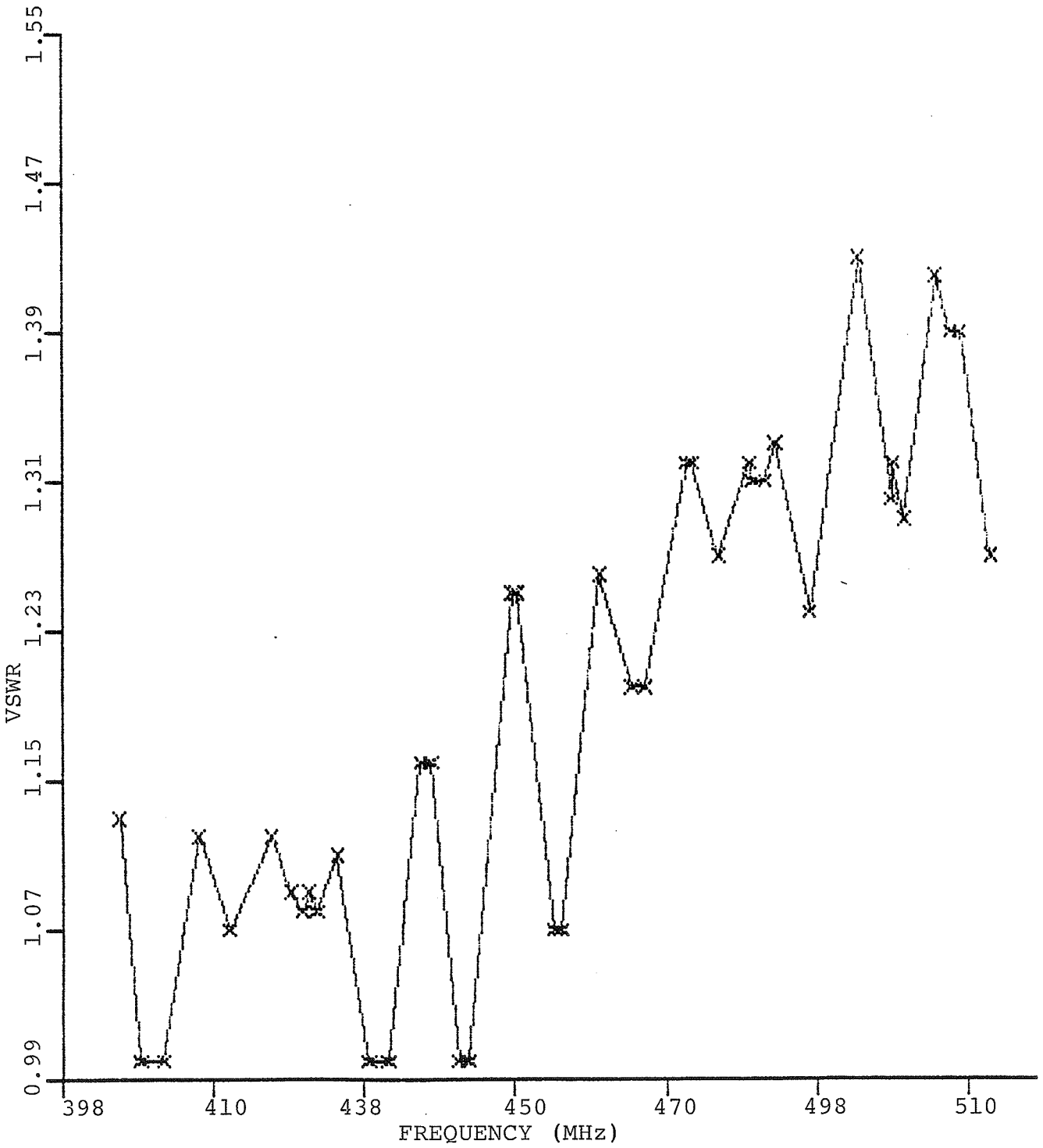

Figure A-1. Frequency Response of the Load.

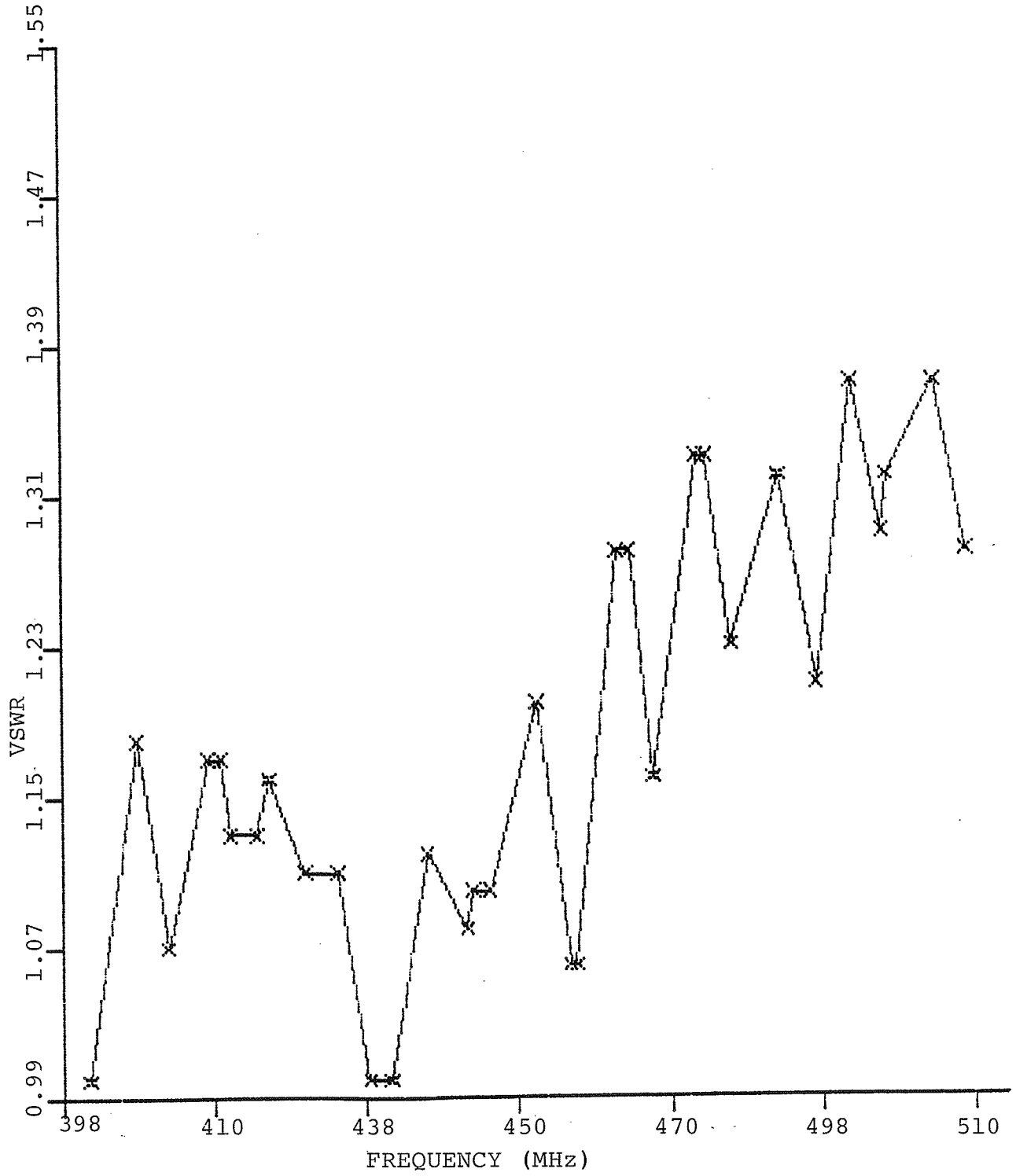

Figure A-2. Frequency Response of Load and Narda Directional Coupler.

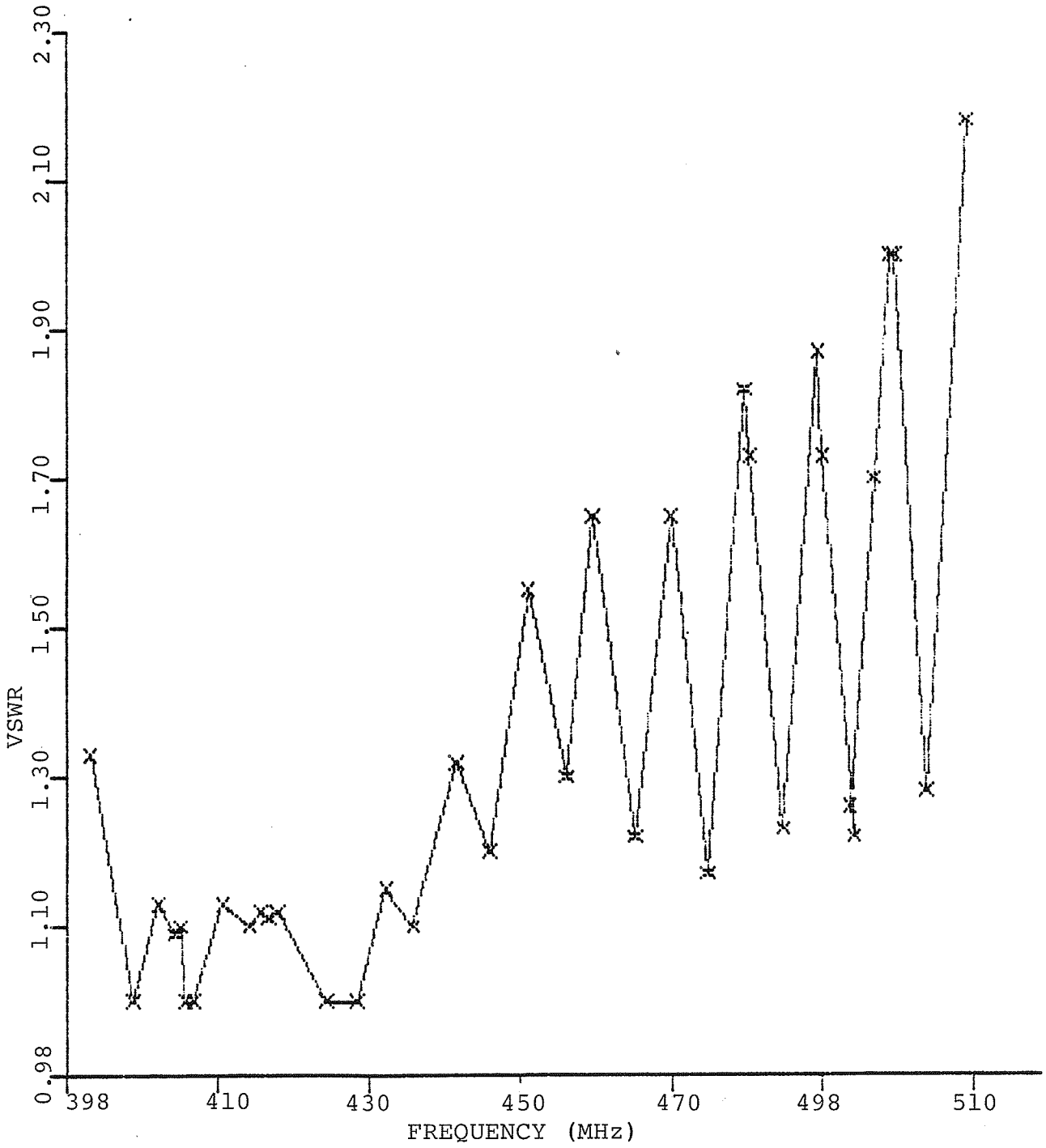

Figure A-3. Frequency Response of Load + Narda Direction Coupler + Crawford Cell.

Table A-1
SARN for the 163.6 Gram Prolate Spheroidal Phantom.
400 MHz, H Polarization. 30 Samples per Data Point.

ECL(%)	SARN(W/kg/mW/cm*cm)	P.D.(mW/cm*cm)
19.09	0.05630	45.233
19.14	0.05352	47.652
19.10	0.05692	45.989
19.09	0.05628	42.751
19.12	0.05592	49.777
19.06	0.06137	51.164
19.11	0.06039	53.932
19.07	0.06534	56.225
19.03	0.05625	43.876
19.08	0.03027	49.865
18.76	0.05692	53.716
18.69	0.06371	58.307
18.63	0.06563	58.663
18.74	0.05744	47.794
18.67	0.05109	42.761
18.51	0.05909	38.018

Table A-2
SARN for the 163.6 Gram Prolate Spheroidal Phantom.
425 MHz, H Polaization 30 Samples per Data Point.

ECL(%)	SARN(W/kg/mW/cm*cm)	P.D.(mW/cm*cm)
2.23	0.08029	52.388
2.20	0.08699	58.349
2.23	0.08052	55.345
2.13	0.07928	46.112
2.05	0.10338	53.967
2.22	0.08209	49.565
2.09	0.08049	43.896
1.98	0.08506	42.399
1.99	0.08100	41.817
2.07	0.08522	44.714
2.26	0.07565	48.389
2.23	0.08378	52.528
2.33	0.07785	56.770
2.29	0.08092	49.714
2.18	0.07625	44.402
1.88	0.08719	38.926

Table A-3
SARN for the 163.6 Gram Prolate Spheroidal Phantom.
450 MHz, H Polarization. 30 Samples per Data Point.

ECL(%)	SARN(W/kg/mW/cm*cm)	P.D.(mW/cm*cm)
11.42	0.09919	46.504
11.16	0.11552	43.557
10.95	0.11803	41.367
11.19	0.11483	45.017
11.32	0.11074	47.736
11.33	0.10961	48.214
11.42	0.10314	49.681
10.70	0.11734	36.512
11.07	0.10663	52.808
10.83	0.11390	45.345
10.86	0.12871	40.948
11.41	0.10211	51.547
11.16	0.07635	44.186
10.48	0.12196	39.416
10.83	0.12208	46.504
11.24	0.10631	43.798

Table A-4
SARN for the 163.6 Gram Prolate Spheroidal Phantom.
475 MHz, H Polarization. 30 Samples per Data Point.

ECL(%)	SARN(W/kg/mW/cm*cm)	P.D.(mW/cm*cm)
14.12	0.11750	46.698
14.09	0.13119	47.593
13.91	0.11058	42.108
13.96	0.07537	41.523
13.84	0.12926	54.555
13.51	0.14128	41.698
13.50	0.12014	42.058
13.52	0.14594	43.087
13.88	0.12313	45.783
13.56	0.10702	35.873
13.74	0.10475	38.417
13.85	0.11485	41.671
14.05	0.12188	47.634
13.95	1.11461	42.878
13.90	0.10362	40.465
14.09	0.12279	49.814

Table A-5
SARN for the 163.6 Gram Prolate Spheroidal Phantom.
500 MHz, H Polarization. 30 Samples per Data point

ECL(%)	SARN(W/kg/mW/cm*cm)	P.D.(mW/cm*cm)
13.08	0.11557	40.796
12.74	0.13481	37.730
12.91	0.11669	37.769
13.18	0.12450	43.401
13.09	0.12860	42.870
12.90	0.14084	39.822
12.73	0.13312	35.908
13.22	0.13920	44.960
12.74	0.12449	32.705
12.96	0.12940	36.524
13.16	0.14302	41.396
13.17	0.15057	42.981
13.21	0.15713	43.982
13.37	0.13667	47.040
12.92	0.14784	35.059
13.00	0.14720	40.805

Table A-6
SARN for the 163.6 Gram Prolate Spheroidal Phantom.
400 MHz, E Polarization. 30 Samples per Data Point.
Small End of Phantom Facing Septum.

ECL(%)	SARN(W/kg/mW/cm*cm)	P.D.(mW/cm*cm)
18.64	0.26778	51.869
18.66	0.27387	46.406
18.71	0.26978	49.051
18.69	0.27066	45.398
18.66	0.27086	43.450
18.71	0.25831	40.855
18.55	0.26824	38.594
18.58	0.27822	53.361
18.46	0.27356	40.970
18.56	0.26861	41.482
18.70	0.25911	43.447
18.69	0.26953	46.217
18.70	0.26107	49.817
18.61	0.27488	51.321
18.64	0.27419	44.545
18.67	0.26873	52.425

Table A-7
SARN for the 163.6 Gram Prolate Spheoidal Phantom.
425 MHz, E Polarization. 30 Samples per Data Point.
Small End of Phantom Facing Septum.

ECL(%)	SARN(W/kg/mW/cm*cm)	P.D.(mW/cm*cm)
2.05	0.40417	42.785
2.05	0.42292	48.545
2.14	0.40884	44.853
2.11	0.41246	46.547
2.09	0.41471	49.547
2.05	0.40358	42.667
2.05	0.41065	44.401
2.10	0.41998	46.139
2.15	0.42516	48.351
2.18	0.40685	48.074
2.22	0.41538	48.903
2.19	0.42518	50.414
1.91	0.40368	38.473
1.95	0.40756	39.764
2.12	0.40845	42.420
2.10	0.42395	45.549

Table A-8
SARN for the 163.6 Gram Prolate Spheroidal Phantom.
450 MHz, E Polarization. 30 Samples per Data Point.
Small End of Phantom Facing Septum.

ECL(%)	SARN(W/kg/mW/cm*cm)	P.D.(mW/cm*cm)
10.59	0.59803	44.928
10.55	0.59388	42.437
10.76	0.59637	48.081
10.69	0.60154	46.637
10.77	0.57609	45.186
10.82	0.58492	46.861
10.63	0.59491	43.447
10.91	0.59168	49.471
10.89	0.58027	45.891
10.78	0.56004	46.793
10.82	0.56666	48.598
10.64	0.57915	43.539
10.97	0.57148	51.598
10.75	0.58892	46.762
10.94	0.57161	52.070
10.71	0.58966	45.852

Table A-9
SARN for the 163.6 Gram Prolate Spheroidal Phantom.
475 MHz, E Polarization. 30 Samples per Data Point.
Small End of Phantom Facing Septum.

ECL(%)	SARN(W/kg/mW/cm*cm)	P.D.(mW/cm*cm)
13.55	1.38853	40.425
13.21	1.39807	38.869
13.41	1.41886	40.911
13.60	1.39291	42.069
13.29	1.43246	41.877
13.09	1.45617	39.219
13.16	1.40617	38.674
13.01	1.33276	36.472
13.28	1.40330	36.826
13.35	1.36217	42.536
13.18	1.38576	39.773
13.43	1.38951	42.841
13.39	1.41620	43.835
13.47	1.42539	45.017
13.43	1.40614	40.874
13.40	1.37991	37.716

Table A-10
SARN for the 163.6 Gram Prolate Spheroidal Phantom.
500 MHz, E Polarization. 30 Samples per Data Point.
Small End of Phantom Facing Septum.

ECL(%)	SARN(W/kg/mW/cm*cm)	P.D.(mW/cm*cm)
12.42	4.81623	33.653
12.85	4.80187	37.022
12.32	4.91518	32.646
12.49	4.87955	34.169
12.64	4.85529	38.286
12.75	4.84990	38.826
12.66	4.87627	37.139
12.79	4.80372	39.776
12.69	4.84320	37.392
12.50	4.89419	35.248
12.85	4.87548	40.420
12.78	4.82820	41.836
12.79	4.84058	43.523
12.68	4.85203	41.319
12.85	4.88350	44.380
12.65	4.97381	39.450

Table A-11
SARN for the 163.6 Gram Prolate Spheroidal Phantom.
400 MHz, E' Polarization. 30 Samples per Data Point.
Small End of Phantom Facing Outer Wall.

ECL(%)	SARN(W/kg/mW/cm*cm)	P.D.(mW/cm*cm)
18.66	0.28420	51.904
18.65	0.28069	50.625
18.67	0.28502	49.522
18.78	0.28409	48.267
18.76	0.29708	47.238
18.83	0.29120	46.372
18.75	0.29135	45.145
18.74	0.28786	44.267
18.77	0.27884	50.175
18.75	0.28232	51.188
18.64	0.27434	49.945
18.71	0.27368	48.825
18.69	0.27159	47.743
18.63	0.27742	46.571
18.65	0.28271	45.472
18.57	0.28545	44.321

Table A-12
SARN for the 163.6 Gram Prolate Spheroidal Phantom.
425 MHz, E' Polarization. 30 Samples per Data Point.
Small End of Phantom Facing Outer Wall.

ECL(%)	SARN(W/kg/mW/cm*cm)	P.D.(mW/cm*cm)
2.27	0.42017	51.908
2.27	0.43458	50.384
2.25	0.42870	48.423
2.23	0.42635	47.461
2.18	0.42205	46.182
2.16	0.42099	45.043
2.01	0.43333	44.341
2.16	0.43476	47.687
2.24	0.42972	51.307
2.11	0.45008	49.776
2.20	0.43343	49.124
2.22	0.42606	47.973
2.18	0.42985	47.350
2.16	0.42782	47.807
2.11	0.43020	44.584
1.99	0.44121	43.794

Table A-13
SARN for the 163.6 Gram Prolate Spheroidal Phantom.
450 MHz, E' Polarization. 30 Samples per Data Point.
Small End of Phantom Facing Outer Wall.

ECL(%)	SARN(W/kg/mW/cm*cm)	P.D.(mW/cm*cm)
11.20	0.58027	53.863
11.17	0.59012	46.392
11.11	0.57738	47.342
11.03	0.59291	44.928
11.03	0.59777	47.653
10.93	0.59291	44.928
10.90	0.58590	43.331
11.08	0.60218	48.977
11.07	0.58239	47.577
11.17	0.58247	50.183
11.17	0.58461	49.374
11.02	0.59121	46.635
10.99	0.58456	45.151
10.82	0.58542	43.181
11.02	0.59890	46.662
11.06	0.61075	49.626

Table A-14
SARN for the 163.6 Gram Prolate Spheroidal Phantom.
475 MHz, E' Polarization. 30 Samples per Data Point.
Small End of Phantom Facing Outer Wall.

ECL(%)	SARN(W/kg/mW/cm*cm)	P.D.(mW/cm*cm)
13.22	1.41985	45.384
13.07	1.44338	41.513
13.15	1.46113	44.577
13.18	1.46292	46.881
13.29	1.43352	47.370
13.19	1.45888	45.614
13.33	1.44274	48.600
13.18	1.45790	44.490
13.47	1.42867	43.938
13.31	1.46209	41.531
13.39	1.45789	46.416
13.31	1.45489	40.552
13.46	1.44280	42.893
13.45	1.43609	43.588
13.45	1.42704	41.965
13.56	1.44530	47.310

Table A-15
SARN for the 163.6 Gram Prolate Spheroidal Phantom.
500 MHz, E' Polarization. 30 Samples per Data Point.
Small End of Phantom Facing Outer Wall.

ECL(%)	SARN(W/kg/mW/cm*cm)	P.D.(mW/cm*cm)
12.58	4.89903	37.588
12.44	4.95065	36.799
12.66	4.97881	37.242
12.80	4.94395	39.102
12.51	4.99483	35.643
12.29	4.99159	33.936
12.84	4.90761	41.040
12.35	4.98297	33.213
12.89	4.90443	41.449
12.97	4.90199	42.759
12.71	4.92454	39.148
12.54	4.99850	34.180
12.66	4.97351	37.787
12.55	4.97128	35.888
12.89	4.93348	40.951
13.14	4.92276	46.172

REFERENCES

1. American National Standards Institute Inc., "Safety Level of Electromagnetic Radiation With Respect to Personnel," New York, New York, 1974.
2. S. M. Michaelson, "Human Exposure to Non-Ionizing Radiant Energy-Potential Hazards and Safety Standards," Proc. IEEE, vol. 60, pp. 389-421.
3. J. C. Lin, A. W. Guy, and C. C. Johnson, "Power Deposition in the Spheriodal Model of Man Exposed to 1-20 MHz Electromagnetic Fields," IEEE Trans. Microwave Theory Tech., vol. MTT-21, pp. 791-797,973.
4. C. C. Johnson, C. H. Duney, and H. Massoudi, "Long Wavelength Electromagnetic Power Absorption in Prolate Spheroidal Models of Man Animals," IEEE Trans. Microwave Theory Tech., vol. MTT-23, pp.739-749, 1979.
5. H. Masoudi, C. H. Durney, and C. C. Johnson, "Long Wavelength Electromagnetic Power Absorption in Ellipsoidal Models of Man and Animals," IEEE Trans. Microwave Theory Tech., vol. MTT-25, pp. 47-52, 1977.
6. D. E. Livesay and K. M. Chen, "Electromagnetic Fields Induced Inside Arbitrarily Shaped Biological Bodies," IEEE Trans. Microwave Theory Tech., vol. MTT-22, pp. 1273-1280, 1974.
7. Electromagnetic Fields in Biological Media, Parts I and II, U. S. Dept. of HEW, Public Health Service, FDA, Aug. 1974.

8. A. Lakhtakia and M. F. Iskander, "Scattering and Absorption Characteristics of Lossy Dielectric Objects Exposed to the Near Field of a Dipole Source," IEEE Trans. Antennas Propagat, vol. AP-31, pp. 111-120, 1983.

9. R. Ruppin, "Calculation of Electromagnetic Energy Absorption in Prolate Spheroids by the Point Matching Method," IEEE Trans. Microwave Theory Tech., vol. MTT-26, pp. 87-90, 1978.

10. R. Kastner, "Spectral Domain Iterative Technique for Analyzing Electromagnetic Scattering from Arbitrary Bodies," Ph.D. Thesis, Dept. of Elect. Eng., University of Illinois, Urbana, IL, 1982.

11. C. H. Durney, "Electromagentic Dosimetry for Models of Humans and Animals: A Review of Theoretical and Numerical Techniques," Proc. IEEE, vol. 68, pp. 33-40, 1980.

12. D. A. Hill, "Human Whole-Body Radio Frequency Absorption Studies Using a TEM-Cell Exposure System," IEEE Trans. Microwave Theory Tech., vol. MTT-30, pp. 33-40, 1980.

13. S. V. Marshall, R. F. Brown, C. H. Hughes, and P. V. Marshall, "An Environmentally Controlled Exposure System for Irradiation of Mice at Frequencies Below 500 MHz," IEEE Internaional Symp. on Electromag. Compat., Boulder, CO., pp. 99-104, Aug, 1981.

14. O. P. Gandhi, "Strong Dependence of Whole Animal Absorption on Polarization and Frequency of Radio Frequency Energy," Annals. NY Acad. Science, vol. 247, pp. 532-538, 1975.

15. O. P. Gandhi, "Conditions of Strongest Electromagnetic Power Deposition in Man Animals" IEEE Trans. Microwave Theory and Tech., vol. MTT-23, pp. 1021-1029, 1975.

16. O. P. Gandhi, "State of the Knowledge for Electromagnetic Absorbed Dose in Man and Animals," Proc. IEEE, vol. 6, pp. 24-32, 1980.

17. M. F. Iskander, H. Massoudi, C. H. Durney, and S. J. Allen, "Measurement of RF Power Absorption in Spheroidal Human and Animal Phatoms Exposed to the Near Field of a Dipole Source," IEEE Trans. BioMed. Eng., vol. BME-28, pp. 258-264, 1981.

18. C. W. Weil and J. B. Kinn, "Advances in Experimental Exposure Methods and Dosimetric Technique Used in Radio-Frequency Biological Effects Study," Proc. IEEE, vol. 71, pp. 222-231, 1983.

19. W. Gee, S. W. Lee, R. Mittra, C. Cain, and R. Magin, "Focused Linear Array for Hyperthermia Research," Sixth Annual Antenna Applications Symposium, Allerton Park, IL., Sept. 1982.

20. R. S. Elliott, W. H. Harrison and F. K. Storm, "Hyperthermia: Electromagnetic Heating of Deep Seated Tumors," IEEE Trans. BioMed. Eng., vol. BME-29, pp. 61-64, 1982.

21. A. W. Guy, "Future Research Directions and Needs in

Biological Electromagnetic Radiation Research," Annals NY Acad. Science, vol. 247, pp. 539-545, 1975.

22. C. C. Johnson, "The Role of Radio Science in Investigating Electromagnetic Biological Hazards," Radio Science, vol. 12, pp. 349-354, 1977.
23. C. C. Johnson and A. W. Guy, "Nonionizing Electromagentic Wave Effects in Biological Materials and Systems," Proc. IEEE, vol. 60, pp. 692-718, 1972.
24. C. H. Durney, C. C. Johnson, P. W. Barber, H. Massoudi, M. Iskander, S. J. Allen, and J. C. Mitchell, Radio Frequency Radiation Dosimetry Handbook, Second Edition, Report SAM-TR-78-72, University of Utah, Salt Lke City, Utah, 1978.
25. Alan Segal, "The Design and Characterization of a Crawford Cell Animal Exposure Facility for Dosimetric Measurements Between 225 to 400 MHz," M.S. Thesis, Dept. of Electrical Eng., University of Illinoi, Urbana, IL. 1981.
26. O. P. Gandhi, Microwave Engineering and Applications, Pergamon Press, New York, 1981.
27. M. L. Crawford, "Generation of Standard EM Fields Using a TEM Transmission Cell," IEEE Trans. Electromag. Compat., pp. 189-195, Nov. 1974.
28. M. L. Crawford, J. L. Workman, and C. L. Thomas, "Expanding the Bandwidth of TEM Cells for EMC Measurements," IEEE Trans. Electromag. Compat., pp. 368-375, Aug. 1978.
29. Greg Pucci, "A Computer Automated Crawford Cell Exposure

System," M.S. Thesis, Dept. of Electrical Eng., University of Illinois, Urbana, IL, 1981.

30. M. L. Crawford, G. A. Hocci, and E. L. Komarek, "RF Differential Power Measurement System for the Brooks AFB Elctromagnetic Radiation Hazard Experiments," NBS Report 9795, Institute of Basic Standards, 1971.

31. A. Von Hippel, Dielectric Materials and Applications, MIT Technology Press, Cambridge, 1954.

32. Handbook of Physics and Chemistry, Chemical Rubber Publishing Company., 57th Edition, 1975.